

Low Tree-Rank Bayesian Vector Autoregression Model

Zeyu Yuwen

Department of Statistics, University of Florida, USA

zeyu.yuwen@ufl.edu

George Michailidis

Department of Statistics, University of Florida, USA

gmichail@ufl.edu

Zhengwu Zhang

Department of Statistics, University of North Carolina, USA

zhengwu_zhang@unc.edu

Leo L. Duan

Department of Statistics, University of Florida, USA

li.duan@ufl.edu

Abstract

Vector autoregressions have been widely used for modeling and analysis of multivariate time series data. In high-dimensional settings, model parameter regularization schemes inducing sparsity have achieved good forecasting performances. However, in many data applications such as those in neuroscience, the graph estimates from existing methods still tend to be quite dense and difficult to interpret, unless we made compromise in the goodness-of-fit. To address this dilemma, in this article we propose to incorporate a commonly used structural assumption — that the ground-truth graph should be largely connected, in the sense that it should only contain at most a few components. We take a Bayesian approach and develop a novel tree-rank prior for the regression coefficients. Specifically, this prior forces the non-zero coefficients to appear only on the union of a few spanning trees. Since each spanning tree connects p nodes with only $(p - 1)$ edges, this prior effectively achieves both high connectivity and high sparsity. In analyzing test-retest functional magnetic resonance imaging data, our model produces a much more interpretable graph estimate, compared to popular existing approaches. In addition, we show appealing properties of this new method, such as differentiable computation, mild stability conditions and posterior consistency.

Keywords: Graph rank, Laplacian matrix, Structural vector autoregression

1 Introduction

Vector autoregression models have been widely used for modeling multivariate time series data in economics Eichler (2007); Maziarz (2015); Stock and Watson (2016), genomics Michailidis and d'Alché Buc (2013); Basu et al. (2015) and neuroscience Seth et al. (2015). The observations $y^t = (y_1^t, \dots, y_p^t) \in \mathbb{R}^p$ at discrete time points $t = 1, \dots, \mathcal{T}$ evolve according to:

$$y^t = C^{(1)}y^{t-1} + C^{(2)}y^{t-2} + \dots + C^{(d)}y^{t-d} + \varepsilon^t, \quad (1)$$

where the transition matrices $C^{(k)} \in \mathbb{R}^{p \times p}$ capture lead-lag effects at lags $1, \dots, d$ and $\varepsilon^t \in \mathbb{R}^p$ is a noise term. The elements of the transition matrices $C^{(k)}$ form a directed graph of Granger causal effects (Granger, 1969); specifically, if there is at least one $C_{i,j}^{(k)} \neq 0$ for some $k = 1, \dots, d$, then it implies that y_j^t is predictive for future values of $y_i^{t'}$ with $t' \geq t + k$, and an edge is included $(j \rightarrow i)$ in the corresponding graph.

However, the dimensionality of the parameter space p^2d and in many applications exceeds the number of available observations. To overcome this challenge, several Bayesian and frequentist regularization approaches have been proposed in the literature. For example, Sims (1989) proposed to impose a Gaussian prior distribution on the elements of the transitions matrices, whereas Banbura et al. (2010) used a Gaussian-inverted Wishart prior distribution to induce ridge type shrinkage. Korobilis (2013) put Bernoulli prior distributions on the indicators of each parameter in the transition matrix to select Granger causal effects. Ghosh et al. (2019) studied the theoretical properties of Bayesian vector autoregressive models under various prior distributions on the parameters and established their posterior consistency. In frequentist approaches, various sparsity inducing penalties have been proposed and studied. Basu and Michailidis (2015) used a lasso penalty and developed key technical results to establish estimation consistency of the model parameters. Variants of sparse regularization schemes were proposed in Kock and Calvet (2015); Lin and Michailidis (2017); Hsu et al. (2008); Nicholson et al. (2020). A different

direction was pursued by Basu et al. (2019) that assumes that the transition matrices exhibit a low-rank and sparse structure. Another variant integrates additional data summarized as factors that incorporated as additional time series in the model (Lin and Michailidis, 2020).

These regularized versions of the vector autoregressive model generally exhibit very good predictive performance. However, in many cases the resulting Granger causal graph is fairly dense which makes interpretation more challenging and/or *disconnected* which contradicts scientific background knowledge in certain applications domains. Indeed, in the neuroimaging application discussed in Section 6 existing sparsity-inducing approaches produce very dense Granger causal graphs, unless the tuning parameters that control the degree of regularization are tuned to produce much sparser estimates at the expense of a significantly poorer goodness-of-fit.

To address this challenge, we introduce a model that posits that the Granger causal graph is (almost) *connected* and contains relatively few edges, thus making it highly interpretable and suitable for applications where the underlying science dictates full connectivity. This is achieved by developing a novel *tree-rank* prior distribution, proposing an algorithm to calculate the posterior distribution of the model parameters and establish its theoretical properties.

The remainder of the paper is organized as follows. In Section 2, we introduce the tree-rank vector autoregression model and develop Gaussian scale mixture prior on the coefficient matrix. In Section 3, we introduce the posterior initialization and computation. In Section 4.1, we prove a mild stability condition for vector autoregression model. In Section 4.2, we establish posterior consistency and model selection consistency. Section 5 and Section 6 illustrate the performance of tree-rank estimates on simulated data and resting-state functional magnetic resonance imaging data, respectively. We conclude with a discussion in Section 7.

2 Modeling Framework

2.1 Vector Autoregressive Processes from a Tree-Covered Graph

The underlying data generating process corresponds to the vector autoregressive model in (1), with $\{C^{(k)}, k = 1, \dots, d\}$ transition matrices defining the Granger causal network $G = (V, E)$ (Basu et al., 2015). Specifically, if there is an edge $(j \rightarrow i) \in E$, then there is at least one $C_{i,j}^{(k)} \neq 0$ for $k = 1, \dots, d$. Further, we assume Gaussian measurement error $\varepsilon^t \stackrel{iid}{\sim} N(0, \Sigma_\varepsilon)$ for all t , for some positive definite covariance Σ_ε .

Next, we incorporate the prior information that G should be sparse and nearly fully connected. Consider the *undirected* version of G , denoted by \bar{G} ; that is, $\bar{G} = \{V, E_{\bar{G}}\}$, with $(i, j) \in E_{\bar{G}}$ if and only if at least one of $(i \rightarrow j)$ or $(j \rightarrow i)$ is in G . We assume that \bar{G} can be covered by m spanning trees,

$$\bar{G} \subseteq \bigcup_{l=1}^m T^l,$$

where the union and subset signs are shorthand for $E_{\bar{G}} \subseteq \bigcup E_{T^l}$ for notational convenience. Recall that a spanning tree T^l is the smallest connected graph containing p nodes, and it has $(p - 1)$ edges. Further, since we assume it to be “connected”, then for any two nodes i and j , there is a set of edges in E_{T^l} (path) that link them together.

To incorporate this structural assumption into the model, we introduce the following Gaussian scale mixture prior distribution:

$$\begin{aligned} C_{i,j}^{(k)} &\stackrel{indep}{\sim} N\{0, \eta_{i,j,k}(r_k \sum_{l=1}^m s_l A_{i,j}^l)^2\}, \\ \eta_{i,j,k} &\stackrel{indep}{\sim} \text{Exp}(\lambda_{i,j,k}^2/2), \quad \lambda_{i,j,k} \stackrel{iid}{\sim} \text{Gamma}(\alpha_\eta, 1), \end{aligned} \tag{2}$$

wherein each $A^l = (A_{i,j}^l)_{i,j=1,\dots,p}$ is the adjacency matrix of a spanning tree T^l , with $A_{i,j}^l = 1$ if $(i, j) \in T^l$, and $A_{i,j}^l = 0$ otherwise. The vector (s_1, \dots, s_m) is a probability vector whose entries add to one, which gives a convex combination of m adjacency matrices. We use

$r_k > 0$ to adjust for the different scales of autoregressive coefficients over $k = 1, \dots, d$.

The above is a global-local parameterization (Polson and Scott, 2010), where the two local scales $(\eta_{i,j,k}, \lambda_{i,j,k})$ can be integrated over to form a generalized double Pareto distribution $\text{GDP}\{0, r_k(\sum_{l=1}^m s_l A_{i,j}^l)/\alpha_\eta, \alpha_\eta\}$ (Armagan et al., 2013):

$$\Pi_0\{C_{i,j}^{(k)} \mid r_k(\sum_{l=1}^m s_l A_{i,j}^l)\} = \frac{1}{2r_k(\sum_{l=1}^m s_l A_{i,j}^l)/\alpha_\eta} \{1 + \frac{|C_{i,j}^{(k)}|}{r_k(\sum_{l=1}^m s_l A_{i,j}^l)}\}^{-(\alpha_\eta+1)}.$$

Effectively, this prior distribution shrinks small coefficients to close to zero, while being tail-robust to large signals.

Since the true order of lags in the vector autoregressive model is unknown, we use a “large” value for the lag order d and make the scale $r_k > 0$ increasingly close to zero for larger values of k , using inverse-gamma prior distributions. Similarly, we use a large value for m , and impose a Dirichlet prior distribution that encourages high sparsity.

$$r_k \stackrel{iid}{\sim} \text{Ga}^{-1}(a_k, b_k), \quad (s_1, \dots, s_m) \sim \text{Dir}(\alpha_s, \dots, \alpha_s).$$

To complete the model description and to facilitate computation of the posterior distribution, we impose a near low-rank structure on the error covariance matrix $\Sigma_\varepsilon = WW^T + I\sigma_\varepsilon^2$, with $W \in \mathbb{R}^{p \times p^*}$ and $p^* < p$. This allows us to use two latent vectors $z^* \sim \text{No}(0, I_{p^*})$ and $\xi \sim \text{No}(0, I_p \sigma_\varepsilon^2)$, and obtain $Wz^* + \xi \sim \text{No}(0, \Sigma_\varepsilon)$. We defer the specification of all the hyper-parameters to the end of Section 2.3.

2.2 Arboricity, Tree Rank and Sub-graph Sparsity

Since the posited prior distribution on $C^{(k)}$ is continuous with the support defined by $\sum_{l=1}^m s_l A_{i,j}^l$, with posterior probability 1, the non-zero elements of $C_{i,j}^{(k)}$ will correspond to the union of m spanning trees. Hence, the associated graph is both connected and exhibits high sparsity with only $m(p - 1)$ edges.

Further, with continuous shrinkage prior distributions on $(r_k, \eta_{i,j,k}, s_l)'s$, some of those non-zero elements $C_{i,j}^{(k)}$ will be in fact very close to zero. Therefore, employing a threshold δ , we have the index set $\{(i, j) : C_{i,j}^{(k)} : |C_{i,j}^{(k)}| \geq \delta \text{ for some } k\}$ correspond to a graph that: (i) can contain disconnected components, and (ii) corresponds to a directed graph as we may have $|C_{i,j}^{(k)}| \geq \delta$ but $|C_{j,i}^{(k)}| < \delta$. Henceforth, we use G (and \bar{G}) to denote the Granger causal graph obtained after thresholding.

Next, we discuss the consequences of covering \bar{G} with m trees. First, note that that the smallest number of trees covering \bar{G} is less or equal to m . This is in fact a summary statistic known as “arboricity”.

$$\arg \min_{m'} \{(T^1, \dots, T^{m'}) : \bar{G} \subseteq \bigcup_{l=1}^{m'} T^l\}.$$

In our setting, it is a hyperparameter that regularizes the prior distribution and henceforth we call it the “tree-rank”. It corresponds to the number of independent factors (spanning trees) that form the basis of a graph (for rigorous definitions of independence in graphs and bases, see Murota (1998)}. Further, we prove that a tree-rank shares a similar range to a matrix-rank.

Theorem 1 *For an undirected graph \bar{G} with p nodes, $1 \leq \text{Tree-Rank}(\bar{G}) \leq p - 1$.*

Therefore, analogously to imposing a low-rank constraint on matrices, a low tree-rank controls the complexity of the graph \bar{G} . However, a key difference with the matrix case is that a low tree-rank m^* automatically ensures a certain level of sparsity, since $|E_{\bar{G}}| \leq m^*(p - 1)$. Further, the tree-rank also induces sparsity in *every* sub-graph of \bar{G} , as shown in the following classical result.

Theorem 2 *Nash-Williams (1964)*

$$\text{Tree-Rank}(\bar{G}) = \max_{H \subseteq \bar{G}} \left\lceil \frac{|E_H|}{|V_H| - 1} \right\rceil. \quad (3)$$

Therefore, with $\text{Tree-Rank}(\bar{G}) \leq m$, we get that every subgraph $H \subset \bar{G}$ has at most $m(|V_H| - 1)$ edges. That is, the tree-rank gives a much stronger control on the sparsity of \bar{G} .

2.3 Prior Distribution on Trees and its Continuous Relaxation

Next, for those adjacency matrices in (2), we specify the prior distribution of the trees that cover the graph \bar{G} . We consider the following form:

$$u_{i,j}^l \stackrel{iid}{\sim} \text{Beta}(a_u, b_u) \text{ for } i < j, \quad u_{i,j}^l = u_{j,i}^l,$$

$$T^l = \arg \max_{\tilde{T}} \sum_{(i,j) \in \tilde{T}} \log u_{i,j}^l.$$

That is, T^l is the maximum spanning tree based on a random symmetric matrix. Since $u_{i,j}^l$'s are independently drawn from a continuous distribution, the maximum spanning tree has a unique solution almost surely.

As each tree is a connected graph, each binary adjacency matrix A^l is subject to a set of complicated constraints, which poses a significant challenge for computation of the posterior distribution. To circumvent this problem, we develop a continuous relaxation for each A^l , denoted by \tilde{A}^l . First, consider an auxiliary spanning tree \tilde{T}^l randomly generated from the following distribution:

$$\text{pr}(\tilde{T}^l; \tau, u^l) = \frac{\prod_{(i',j') \in \tilde{T}^l} (u_{i',j'}^l)^{1/\tau}}{\sum_{\text{all } \tilde{T} \in \mathbb{T}} \prod_{(i',j') \in \tilde{T}} (u_{i',j'}^l)^{1/\tau}}, \quad (4)$$

where \mathbb{T} is the space of all spanning trees with p nodes and $\tau > 0$ a tuning parameter that controls the degree of relaxation. Set

$$\tilde{A}_{i,j}^l = \text{pr}\{\tilde{T}^l \ni (i,j); \tau\} = \sum_{\text{all } \tilde{T}^l \in \mathbb{T}} \{(i,j) \in \tilde{T}^l\} \text{pr}(\tilde{T}^l; \tau, u^l).$$

as the marginal probability for \tilde{T}^l to include the edge (i,j) . Together, we obtain a matrix of marginal probabilities $\tilde{A}^l = (\tilde{A}_{i,j}^l)_{i,j=1,\dots,p}$. This matrix in fact has a closed-form solution (Duan and Dunson (2021, arXiv preprint 2106.16120) and Schwaller et al. (2019)):

$$L_{i,j} = \begin{cases} \sum_{k \neq i} (u_{i,k}^l)^{1/\tau} & \text{if } i = j, \\ -(u_{i,j}^l)^{1/\tau} & \text{if } i \neq j. \end{cases} \quad \tilde{A}_{i,j}^l = (u_{i,k}^l)^{1/\tau} \frac{\partial \log\{\text{cofactor}_{1,1}(L)\}}{\partial \{(u_{i,k}^l)^{1/\tau}\}}, \quad (5)$$

which can be efficiently computed using auto-differentiation software in Paszke et al. (2017). In the above, L is often referred to as the graph Laplacian, and $\text{cofactor}_{1,1}(L)$ is the cofactor equal to the determinant of the submatrix of L removing its first row and column.

To show that \tilde{A}^l is a relaxation of A^l , note that when $\tau \rightarrow 0$, the distribution (4) converges to a point mass at the maximum spanning tree T^l . Therefore, $\tilde{A}_{i,j}^l \rightarrow 1$ if $(i,j) \in T^l$, and $\tilde{A}_{i,j}^l \rightarrow 0$ otherwise. Using \tilde{A}^l in place of A^l at a small but non-zero τ , leads to the log-posterior distribution becoming continuous and differentiable in u^l . This allows us to use gradient-based computation and Hamiltonian Monte Carlo for its computation.

Next, we specify the hyper-parameters mentioned above. First, we standardize each vector (y_j^1, \dots, y_j^T) so that it has sample mean 0 and sample variance 1. This allows us to set the noise variance roughly on the same scale, $\sigma_\varepsilon^2 \sim \text{Gamma}^{-1}(2, 1)$ and $W_{i,j} \sim \text{No}(0, 1)$. Next, for the generalized double Pareto distribution, we follow Armagan et al. (2013) and use $\alpha_\eta = 3$ to balance between sparsity and tail-robustness. To regularize the order of autoregression, we use $a_k = 3$ and $b_k = 2 \cdot 0.1^k$, corresponding to increasingly smaller prior mean $\mathbb{E}r_k = 0.1^k$ and variance $\mathbb{V}r_k = 0.1^{2k}$ as k increases. Similarly, we set $\alpha_s = 0.1$ to encourage sparsity in the Dirichlet distribution for s_l . For the tree prior, we use $a_u = 1$ and $b_u = 1$, so that $-\log(u_{i,j}^l)/\tau$ follows an exponential distribution with mean $1/\tau$. We use $\tau = 0.01$ as it enjoys a good balance between binary approximation and non-trivial gradient in computation.

3 Computing the Posterior Distribution

3.1 Hamiltonian Monte Carlo

We use the Hamiltonian Monte Carlo algorithm Neal (2010) for this task and provide the necessary details pertaining to the posited model.

To sample the parameter θ from target posterior distribution $\theta \sim \Pi_{\theta|y}(\cdot)$, Hamiltonian Monte Carlo uses an auxiliary momentum variable v with density $\Pi_v(v)$, and samples from joint distribution $\Pi(\theta, v) = \Pi_{\theta|y}(\theta)\Pi_v(v)$. The potential and kinetic energies are defined as $U(\theta) = -\log \Pi_{\theta|y}(\theta)$ and $K(v) = -\log \Pi_v(v)$, with total Hamiltonian energy $H(\theta, v) = U(\theta) + K(v)$. We select a common quadratic kinetic energy $K(v) = v^T M v / 2$ with M being positive definite, and potential energy as the log-posterior density,

$$\begin{aligned} U(\theta) = & \frac{(\mathcal{T} - d)p}{2} \log \sigma_\varepsilon^2 + \frac{1}{2\sigma_\varepsilon^2} \|Y - X\bar{C} - Z^*W^T\|_F^2 + 3 \log(\sigma_\varepsilon^2) + 1/\sigma_\varepsilon^2 \\ & + \sum_{i,j,k} \left[(\alpha_\eta + 1) \log \left\{ 1 + \frac{|C_{i,j}^{(k)}|}{r_k(\sum_{l=1}^m s_l \tilde{A}_{i,j}^l)} \right\} + \log \left\{ r_k \left(\sum_{l=1}^m s_l \tilde{A}_{i,j}^l \right) \right\} \right] - \sum_{l=1}^m \log J(U^l, \tilde{A}^l) \\ & - \sum_{l=1}^m (\alpha_s - 1) \log(s_l) + \sum_{k=1}^d \left\{ (a_k + 1) \log r_k + b_k/r_k \right\} + \|W\|_F^2/2 + \|Z^*\|_F^2/2 \\ & - \sum_{l=1}^m \sum_{i < j} \left\{ (a_u - 1) \log(u_{i,j}^l) + (b_u - 1) \log(1 - u_{i,j}^l) \right\} + \text{constant}, \end{aligned}$$

where $J(U^l, \tilde{A}^l)$ is the determinant of the Jacobian matrix of partial derivatives of \tilde{A}^l with respect to $U^l = (u_{i',j'}^l)_{\text{all } i,j}$. Denote by: $Y = [y_{\mathcal{T}}^T, \dots, y_{d+1}^T] \in \mathbb{R}^{(\mathcal{T}-d) \times p}$, $\bar{C} = [C^{(1)T}, \dots, C^{(d)T}] \in \mathbb{R}^{(pd) \times p}$, $X = \begin{bmatrix} y_{\mathcal{T}-1}^T & \dots & y_{\mathcal{T}-d}^T \\ \vdots & \ddots & \vdots \\ y_d^T & \dots & y_1^T \end{bmatrix} \in \mathbb{R}^{(\mathcal{T}-d) \times (pd)}$ and $Z^* \in \mathbb{R}^{(\mathcal{T}-d) \times p^*}$.

At each state (θ, v) , ideally, a new state (θ^*, v^*) can be generated by simulating Hamiltonian dynamics that satisfy Hamilton's equations:

$$\frac{\partial \theta}{\partial t} = \frac{\partial H(\theta, v)}{\partial v} = Mv, \quad \frac{\partial v}{\partial t} = -\frac{\partial H(\theta, v)}{\partial \theta} = -\frac{\partial U(\theta)}{\partial \theta}. \quad (6)$$

Since the exact solution of (6) is intractable, it is common to approximate solutions using a leapfrog scheme via

$$v \leftarrow v - \frac{\epsilon}{2} \frac{\partial U(\theta)}{\partial \theta}, \quad \theta \leftarrow \theta + \epsilon Mv, \quad v \leftarrow v - \frac{\epsilon}{2} \frac{\partial U(\theta)}{\partial \theta}. \quad (7)$$

The proposal (θ^*, v^*) is generated by taking \mathcal{L} leapfrog steps from the current state $(\theta^{(0)}, v^{(0)})$,

and accepted using the Metropolis-Hastings criterion with probability:

$$\min\{1, \exp[-H(\theta^*, v^*) + H(\theta^{(0)}, v^{(0)})]\}.$$

Despite the involved expression of the potential energy $U(\theta)$, we can nevertheless evaluate all terms and the Jacobian in its specification, as well as the gradient $\partial U(\theta)/\partial\theta$ easily. This task can be accomplished by leveraging the automatic differentiation capability in the PyTorch package, as well as the automatic tuning of ϵ and L in the above leapfrog scheme in the `hamiltorch` package Cobb and Jalaian (2021).

3.2 Initialization via Bi-convex Optimization

For an efficient exploration of the high posterior density region, especially under a high dimensional model not possessing a log-concave density, a good initialization of the Markov chain is required.

Note that $U(\theta)$ is a non-convex function and likely has multiple local optima. In order to rapidly obtain reasonable initial values on the tree covering and \bar{C} , we consider the following simpler optimization problem, as an approximation (note that this also gives a simpler low-tree rank model that may be of independent interests):

$$\begin{aligned} & \min_{\bar{C}, Z, \cup_{l=1}^m T^l} \frac{1}{2} \|(Y - X\bar{C})\|_F^2 + \frac{\rho}{2} \|\bar{C} - Z\|_F^2 + \rho \text{tr} \Psi^T (\bar{C} - Z) \\ & \text{subject to } Z_{i,j}^{(k)} = 0 \text{ if } (i, j) \notin \cup_{l=1}^m T^l, \\ & \quad T^l \cap T^{l'} = \emptyset \text{ for } l \neq l', \end{aligned} \tag{8}$$

where we use the splitting technique so that $\bar{C} = Z$ at the optimum. Note that \bar{C} and Z can be updated alternatively in simple form. Further, $\rho > 0$ is a split parameter (which does not impact the optimal solution), and Ψ is a $(pd) \times p$ matrix containing the Lagrange multipliers of the constraints in (8). Using the alternating direction method of multipliers, we can minimize the

objective function in (8) by iteratively updating the three parameters as follows:

$$\bar{C} \leftarrow (X^T X + \rho I)^{-1} (X^T Y + \rho Z - \rho \Psi),$$

$$Z \leftarrow \hat{A}^* \circ (\bar{C} + \Psi),$$

$$\Psi \leftarrow \Psi + \bar{C} - Z,$$

where \hat{A}^* is the binary adjacency matrix of $\cup T^{l*}$ corresponding to finding the top m disjoint spanning trees:

$$\arg \max_{T^1, \dots, T^m: T^l \cap T^{l'} = \emptyset} \sum_{l=1}^m \sum_{(i,j) \in T^l} [(\bar{C} + \Psi)_{i,j}^{(k)}]^2,$$

which can be solved efficiently using Prim's algorithm (Prim, 1957) m times.

The optimization problem in (8) is bi-convex; it is convex in \bar{C} given $\cup_l^m T^l$, and M-convex in $\cup T^l$ given \bar{C} {M-convexity is the discrete extension of continuous convexity, see Murota (1998)}. For this type of problem, typically one only needs a good starting value so that the algorithm can converge to the global optimum. In this case, we use the l_2 -regularized estimator $(X^T X + I)^{-1} (X^T Y)$ as the starting value for \bar{C} , and we found that empirically it leads to satisfactory convergence. After the optimization of \bar{C} , we fix \bar{C} and minimize $U(\theta)$ over the other parameters using a gradient descent algorithm. This algorithm enjoys a fast convergence rate, and empirically the solution of the optimization problem takes less than two minutes on an quad-core laptop for each example presented in this article.

3.3 Choosing Sufficiently Large d and m via the Plateau Method

Recall that it is preferable to set the parameters m and d to large values, which in turn would increase the computational cost of the algorithm. To overcome this challenge, we leverage the fast convergence of the above optimization algorithm and develop an empirical plateau method that allows to quickly select m and d to be sufficiently large.

When d and m increase, the optimized loss function in (8) is guaranteed to decrease; on the other hand, the rate of change will slow down after they go above certain threshold. Following the popular “elbow method” in selecting number of factors in principal component analysis (Cattell, 1966), we use a two-dimensional extension that we call “plateau method”. That is, we obtain optimized values over a range of (d, m) , and find where these values start to become close to a flat surface — importantly, in high-dimensional setting, as the linear system is under-determined, (8) would go to zero with large d and m , hence this surface is close to a zero-valued plane.

To obtain an automated algorithm, we use an approach similar to Li and Pati (2017) — we divide the minimized loss values into two groups using K -means algorithm with $K = 2$, then find the smallest (m, d) in the group with the mean closer to zero. We plot the result for visualization and diagnostics. As shown in Figure 1 (associated with our data application), the algorithm lead us to choose $(d, m) = (2, 2)$.

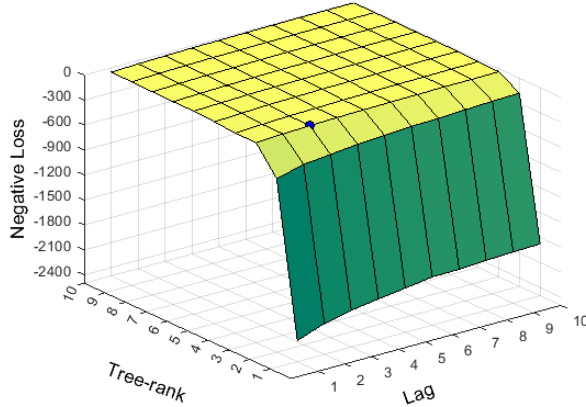


Figure 1: Three dimensional plot of negative minimized loss versus lag d and tree-rank m . The optimized loss approaches zero-valued plateau as d and m increase, allowing us to choose a small (d, m) [(2, 2) in this case] to ensure both good fitting and parsimony.

4 Consistency of Low Tree-Rank Vector Autoregression Models

4.1 Stability Condition

A sufficient condition for vector autoregression model to be stable (Lütkepohl, 2005) is that for any complex scalar $z \in \mathbb{C}$: $|z| \leq 1$,

$$\det(I_p - C^{(1)}z - \dots - C^{(d)}z^d) \neq 0. \quad (9)$$

Next, we derive an easy to verify sufficient condition. Note that we can view $A(C, z) := C^{(1)}z + \dots + C^{(d)}z^d$ as a complex-valued and weighted adjacency matrix for a graph, where the weights correspond to the transition matrices $C^{(k)}$, $k = 1, \dots, d$. Since the graph Laplacian matrix is by construction positive semi-definite, we can enforce $\det\{I_p - A(C, z)\} > 0$.

Theorem 3 *Consider two transformed matrices of $C^{(1)}, \dots, C^{(d)}$ that are real-valued and symmetric:*

$$(\tilde{A}^*)_{i,j} = \left[\sum_{k=1}^d \left\{ \frac{C_{i,j}^{(k)} + C_{j,i}^{(k)}}{2} \right\}^2 \right]^{1/2}, \quad (\tilde{A}^{**})_{i,j} = \left[\sum_{k=1}^d \left\{ \frac{C_{i,j}^{(k)} + g_0 C_{j,i}^{(k)}}{2} \right\}^2 + (1 - g_0^2) \left\{ \frac{C_{j,i}^{(k)}}{2} \right\}^2 \right]^{1/2}$$

for $i = 1, \dots, p$ and $j = 1, \dots, p$, with $g_0 = -0.4 - 0.61/d$. Then, a sufficient condition for the vector autoregressive process (1) to be stable is that for all i , the node degrees

$$\tilde{D}_i^* = \sum_{j=1}^p (\tilde{A}^*)_{i,j} < 1/\sqrt{d}, \quad \tilde{D}_i^{**} = \sum_{j=1}^p (\tilde{A}^{**})_{i,j} < 1/\sqrt{d}.$$

Remark 1 This result holds for any vector autoregressive process, although it is particularly meaningful for low tree-rank and/or sparse models. Since each node is only connected to a few edges, hence most of $(C_{i,j}^{(k)}, C_{j,i}^{(k)})$'s are zero, making the above condition easy to satisfy. A similar, but necessary condition was derived in Proposition 2.2 (i) of Basu and Michailidis (2015) that assumes (9) to be true. Therefore, our new result shows that stability can be achieved via the sparsity condition, in addition to the well known spectral radius condition $\|C^{(1)}\| < 1$ for an order-1 vector autoregression (Loh and Wainwright, 2012).

4.2 Consistency

Next, we derive conditions for consistent estimation of the elements of the transition matrices, as the number of observations $\mathcal{T} \rightarrow \infty$. First, we rewrite the model in a linear regression form as

$$Y = XC + \mathcal{E}, \quad (10)$$

where $\mathcal{E} := [\varepsilon^T, \dots, \varepsilon^{d+1}]_{N \times p}^T$ is the error matrix.

We assume that observations are generated according to (1) with ground-truth $C_0 = \{C_0^{(1)}, \dots, C_0^{(d)}\}^T$, and associated ground-truth graph \bar{G}_0 . For ease of presentation, we denote with $N := \mathcal{T} - d$ and use vectorized notation for $c = \text{vec}(C)$, $y = \text{vec}(Y)$, $c_0 = \text{vec}(C_0)$, and (i, j, k) as a shorthand for the corresponding vectorized single index $kp^2 + jp + i$. Then, the likelihood function of model (1) is given by

$$\mathcal{L}(y; c, \Sigma_\varepsilon) \propto \det(\Sigma_\varepsilon)^{-\frac{\mathcal{T}-d}{2}} \exp\left[-\frac{1}{2}\{y - (I_p \otimes X)c\}^T (\Sigma_\varepsilon \otimes I_{T-d})^{-1} \{y - (I_p \otimes X)c\}\right].$$

The prior distribution on c is $c \sim \text{No}(0, \Phi)$, with $\Phi = \text{diag}\{\eta_{i,j,k}(r_k \sum_{l=1}^m s_l A_{i,j}^l)^2\}$. This is based on the first line of (2), where c follows a Gaussian scale mixture prior.

The conditional posterior distribution is then given by

$$\begin{aligned} (c \mid \Sigma_\varepsilon, r, \eta, s, A) &\sim \text{No}\{\hat{c}, (\hat{\Gamma} + \Phi^{-1}/N)^{-1}/N\} \\ \hat{c} &= (\hat{\Gamma} + \frac{\Phi^{-1}}{N})^{-1} \hat{\gamma}, \\ \hat{\Gamma} &= \Sigma_\varepsilon^{-1} \otimes X^T X/N, \quad \hat{\gamma} = (\Sigma_\varepsilon^{-1} \otimes X^T) y/N. \end{aligned} \quad (11)$$

Next, we impose certain assumptions on X, \mathcal{E} and some of the hyperparameters.

(A1) Deviation condition: there exists a deterministic function $\mathbb{Q}(c_0, \Sigma_\varepsilon)$,

$$\|X^T \mathcal{E}/N\| \leq \mathbb{Q}(c_0, \Sigma_\varepsilon) \sqrt{p/N}. \quad (12)$$

(A2) The value r_k , s_l and $\eta_{i,j,k}$ are bounded from below at a constant that does not change with N, p , almost everywhere with respect to the posterior probability; whereas $A_{i,j}^l \in (\epsilon, 1)$. As $\tau \rightarrow 0, \epsilon \rightarrow 0$ uniformly for any N, p .

(A3) $0 < \inf_{N \geq 1} \lambda_{\min}(C_X) < \infty$, $0 < \sup_{N \geq 1} \lambda_{\max}(C_X) < \infty$, where C_X is the covariance matrix of each row of the data matrix X .

(A4) $\|c_0\| \leq K$, where K is a positive constant.

(A5) $\lambda_{\min}(\Sigma_\varepsilon) > 0, \lambda_{\max}(\Sigma_\varepsilon) < \infty$.

By Corollary B.4. of Ghosh et al. (2019), $\|X^T E/N\| \leq 4\mathbb{Q}_1(c_0, \Sigma_\varepsilon)\{p(d+1) \log 21/N + \sqrt{p/N}\}/\zeta$ with probability at least $1 - 6\exp\{-\sqrt{Np}\}$, where $\mathbb{Q}_1(c_0, \Sigma_\varepsilon)$ is a deterministic function and ζ is a positive constant. For sufficiently large N , we can have $\|X^T E/N\| \leq 8\mathbb{Q}_1(c_0, \Sigma_\varepsilon)\sqrt{p/N}/\zeta$. This implies Assumption A1 holds with high probability for large N , where $\mathbb{Q}(c_0, \Sigma_\varepsilon)$ in (12) can be chosen as $8\mathbb{Q}_1(c_0, \Sigma_\varepsilon)/\zeta$. Moreover, Assumption A1 leads to $\|X^T E/N\|_F \leq \mathbb{Q}(c_0, \Sigma_\varepsilon)\sqrt{dp^2/N}$ and note that $\hat{\gamma} - \hat{\Gamma}c_0$ is precisely $\text{vec}(X^T E/N)$, which ensures $\|\hat{\gamma} - \hat{\Gamma}c_0\|$ converges to 0 as $N \rightarrow \infty$.

Assumption A2 ensures the boundedness of $\|\Phi^{-1}\|$, which plays an important role in the consistency proof. Assumptions A3 and A5 are standard ones in vector autoregression models and ensure that $\lambda_{\min}(X^T X/N)$ is bounded away from 0 and $\lambda_{\max}(X^T X/N)$ is bounded above with high probability.

Assuming $\bigcup_{l=1}^m T^l \not\supseteq \bar{G}_0$, we establish that the posterior probability of such T_l 's goes to 0 as $N \rightarrow \infty$. In order to do so, we compare posterior densities $\mathbb{P}_0(\Phi_* \mid y, X)$ and $\mathbb{P}_0(\Phi_{**} \mid y, X)$, where Φ_* is the Gaussian scale parameter corresponding to a set of trees $\bigcup_{l=1}^m T_*^l \supseteq \bar{G}_0$ and Φ_{**} corresponding to a set of trees $\bigcup_{l=1}^m T_{**}^l \not\supseteq \bar{G}_0$.

Theorem 4 Consider a stable vector autoregressive model with true parameter c_0 of tree-rank

m satisfying A1-A6, for every $\eta > 0$. Then, posterior consistency holds, since

$$\mathbb{P}_0\{||c - c_0|| > \eta \mid \Phi, y, X\} \rightarrow 0, \text{ as } N \rightarrow \infty. \quad (13)$$

Moreover, we have

$$\mathbb{P}_0(\Phi_{**} \mid y, X) / \mathbb{P}_0(\Phi_* \mid y, X) \xrightarrow{P_0} 0, \text{ as } N \rightarrow \infty, \quad (14)$$

where Φ_* corresponds to a set of trees $\bigcup_{l=1}^m T_*^l \supseteq \bar{G}_0$ and Φ_{**} corresponds to a set of trees $\bigcup_{l=1}^m T_{**}^l \not\supseteq \bar{G}_0$.

Remark 2 The first result shows that the posterior distribution concentrates around the true parameter c_0 , while the second one establishes a posterior ratio consistency for the trees covering the ground-truth graph \bar{G}_0 hence model selection consistency. In the Supplementary Materials, we further characterize the convergence rate when Φ_* covers \bar{G}_0 .

5 Performance Evaluation

We assess the finite sample performance of the model and the estimation procedure for a finite \mathcal{T} varying between 200 and 1600, and for $p = 30$ and 80. We experiment with two types of ground-truth Granger causal graphs G_0 : (i) a low tree-rank one, and (ii) a random sparse graph. The former is used to empirically show fast convergence of the posterior distribution, while the latter is to assess the robustness of the posited model when the ground-truth deviates from it.

For each G_0 , with $d = 1$, we randomly generate a transition matrix C_0 with $C_{0:i,j}^{(k)}$ from $\text{No}(0, 1)$ if $(i, j) \in \bar{G}_0$, and $C_{0:i,j}^{(k)} = 0$ otherwise, then scaled down to satisfy the stability condition in Theorem 3. We use a covariance matrix $\Sigma_\varepsilon = \tilde{\rho}(0.5^{|i-j|})_{i,j=1,\dots,p}$, and then scale $\tilde{\rho}$ such that the signal-to-noise ratio $||C_0||_F / ||\Sigma_\varepsilon||_F = 2$.

For comparison purposes, we employ a regularized vector autoregression model based on a lasso with their tuning parameters estimated using cross-validation, as implemented in the `scikit-learn` package.

We assess the performance of our model on the following tasks: (i) recovering the support of \bar{G}_0 , (ii) assessing the estimation error $\|\hat{C} - C_0\|_F / \|C_0\|_F$ with \hat{C} the posterior mean, and (iii) assessing the prediction error $\|Y^* - \hat{Y}^*\|_F / \|Y^*\|_F$, with \hat{Y}^* the sample mean of simulated Y^* 's, with one \hat{Y}^* generated from (1) given each posterior sample of (C, Σ_ε) . The results are based on 50 replicates.

We first consider the case where \bar{G}_0 is indeed a graph of low tree-rank set to 2. The tree-rank regularized model shows a rapid drop in the estimation error even at small \mathcal{T} , as well as good prediction performance (Figure 2).

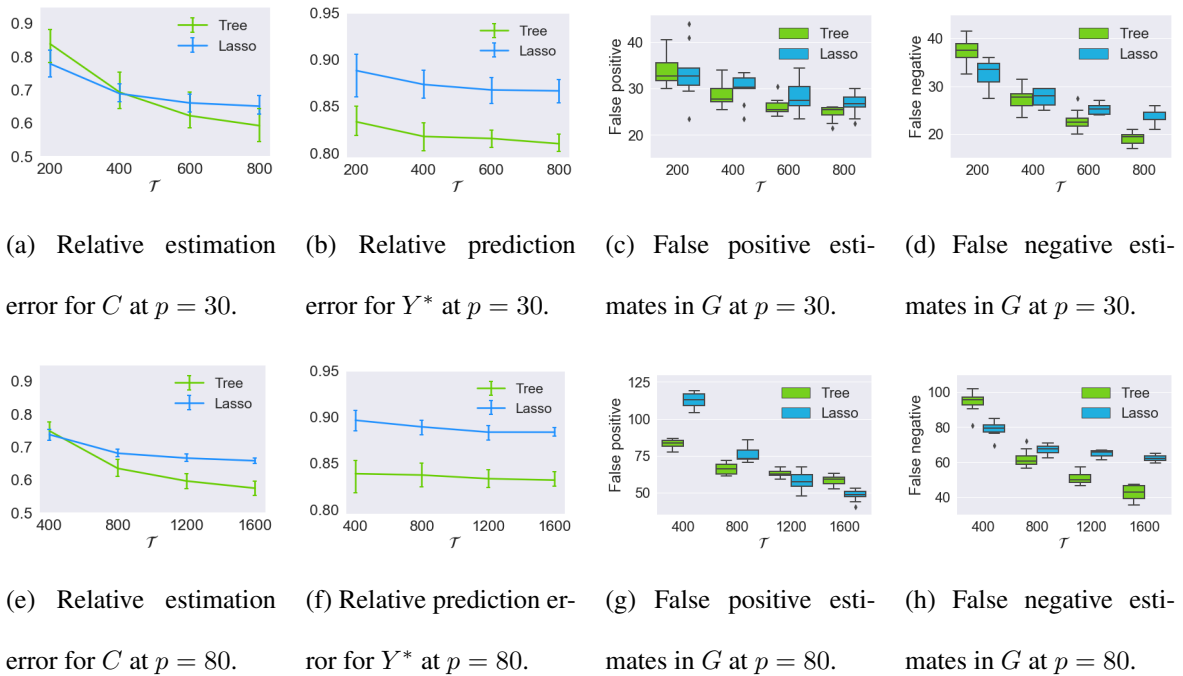


Figure 2: Simulation results when the ground-truth graph \bar{G}_0 has a low tree-rank at 2.

We next explore the case where \bar{G}_0 is an unstructured sparse graph. We generate adjacency matrices A_0 's with about $5\%p(p-1)/2$ edges at random. Similarly to the first case, our model

again shows good performance in terms of estimation and prediction (Figure 3).

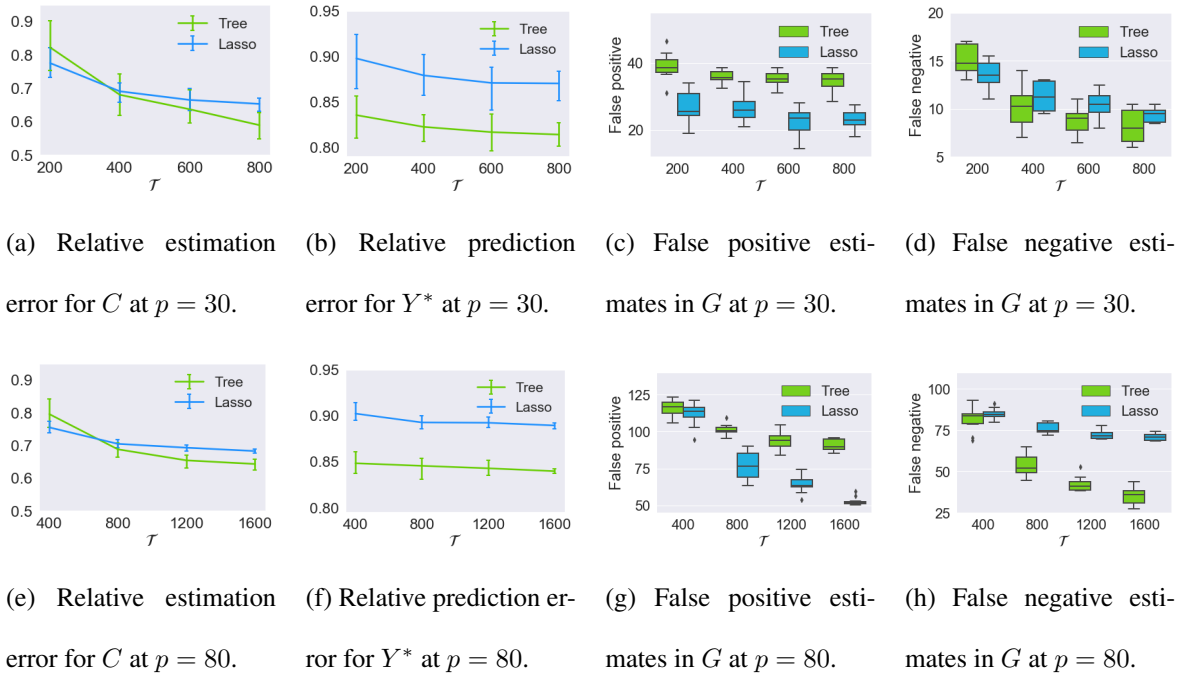


Figure 3: Simulations when the ground-truth graph \bar{G}_0 is unstructured and 95% sparse.

Lastly, in the above simulations, note that the true underlying tree-rank of G_0 is known. We use $\sum_{l=1}^m 1(s_l > 10^{-5})$ as an effective tree-rank estimate based on each posterior sample, then combine those estimates to quantify the posterior distribution of the tree-rank. Figure 4 provides an illustration from one simulation with $p = 80$. Among all the experiments, we find that approximate 60% of times we have the posterior mode of effective tree-rank exactly equal to the one in G_0 .

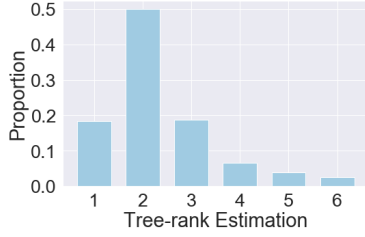


Figure 4: Posterior distribution of the effective tree-rank $\sum_{l=1}^1 (s_l > 10^{-5})$ when Tree-Rank(\bar{G}_0) = 2.

6 Application to Neuroimaging Data Analysis

We employ the proposed model to analyze resting-state functional magnetic resonance imaging (fMRI) data from the Human Connectome Project. The fMRI data contain the blood oxygen level-dependent (BOLD) signals for $\mathcal{T} = 1200$. We use average BOLD signals in 68 brain cortical regions of interest according to the Desikan-Killarney atlas (Desikan et al., 2006). We use ten subjects, with each having two scans: “test” scan from a first visit and another “retest” scan from a follow-up visit.

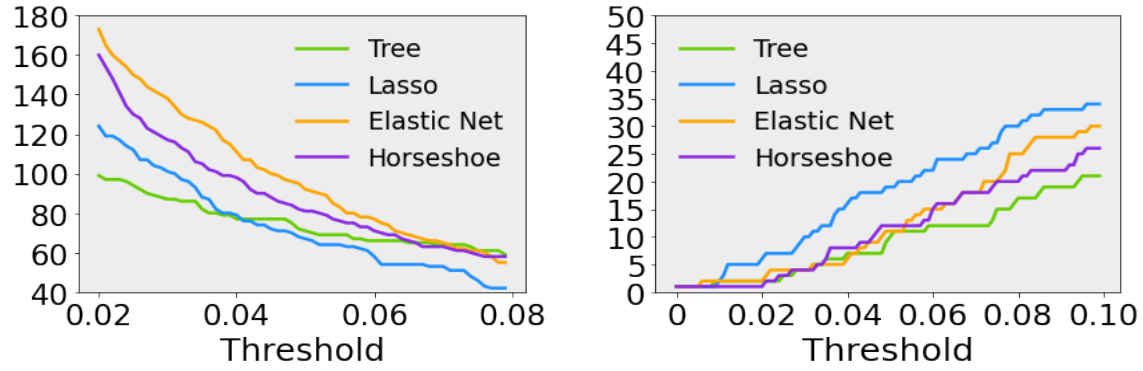
As a study focusing on reproducibility, we use test scans as the training data for graph estimation, and retest scans as validation dataset to assess how many edge estimates can be reproduced. Using Desikan et al. (2006), we divide the 68 regions into 6 larger cortical regions: front lobe, insula, cingulate, parietal lobe, temporal lobe and occipital lobe.

We fit our model by running the Markov chain Monte Carlo sampler for 5,000 iterations, and discard the first 2,500 as the burn-in. We set the hyper-parameters according to Section 2, with $(m, d) = (2, 2)$ using the plateau method. To produce an interpretable point estimate for G , we use the posterior mean \bar{C} and threshold them to obtain edge set $\{(i, j) : \bar{C}_{i,j}^{(k)} : |\bar{C}_{i,j}^{(k)}| \geq \delta \text{ for some } k\}$.

For comparison, we also fit sparse vector autoregression models employing (i) lasso regular-

ization, (ii) a horseshoe prior distribution for the model parameters Carvalho et al. (2010) and (iii) elastic net regularization. For (i) and (iii), we use cross-validation to tune the penalty parameter; for (ii), following the default choice, we use a half Cauchy prior distribution scaled by σ_ε^2 for the global scale parameter.

Clearly, the number of edges in the estimated graph is sensitive to the chosen threshold. Therefore, we plot the number of edges versus the threshold in Figure 5(a). It can be seen that the low tree-rank model produces a graph with the smallest number of edges at small $\delta \in (0.02, 0.04)$. Notably in this range of δ , each corresponding graph contains the smallest number of disconnected components among all. The horseshoe prior model shows a similar result on the number of components, except that it contains more edges. Therefore, these two graphs have a higher connectivity compared to the ones from lasso and elastic net.



(a) The number of edges versus threshold δ (0-0.02) omitted due to the scales are too large). (b) The number of disconnected components versus threshold δ .

Figure 5: Comparing the number of edges and disconnected components of graph estimates from different autoregressive models.

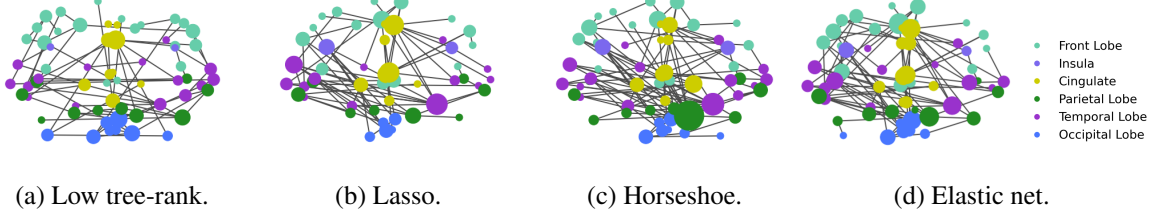


Figure 6: Comparing graph point estimates from several vector autoregressive models. Nodes are plotted using the Desikan-Killiany atlas node coordinates and sized according to their degrees. Six cortical regions are shown in colors. For a more clear visualization, we use a higher threshold at $\delta = 0.045$.

	Low tree-rank	Lasso	Horseshoe	Elastic net
Fitted R^2 on “test” data	0.9946	0.8352	0.9922	0.8384
Validation R^2 on “retest” data	0.9933	0.7903	0.9816	0.7917

Table 1: Goodness of fit in R^2 for the training “test” data and validation “retest” data.

Next, we examine the reproducibility of graph estimation, by taking the fitted \hat{C} to the “retest” dataset, and then compute the coefficient of determination R^2 . As shown in Table 1, in terms of fitting the training data, all four models show excellent R^2 ; however, when it comes to the validation set, the lasso and elastic net based estimates suffer from a significant drop in R^2 .

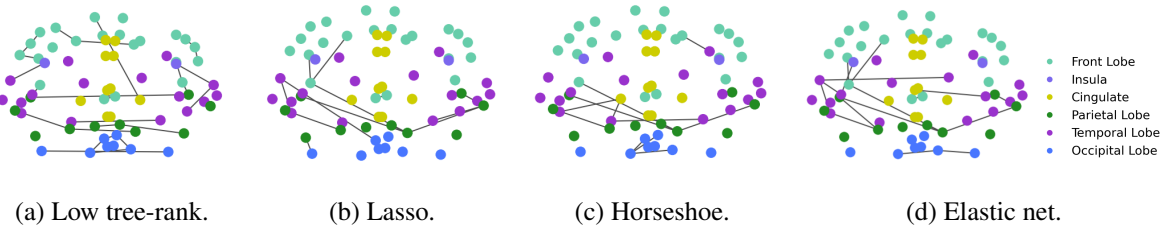


Figure 7: Visualization of the “reproduced edges”, as the same edges estimated from two model fitting to the “test” and “retest” datasets.

To find out the reasons for such differences, we retrain these four models on the “retest” dataset, obtain the graph estimates, and compare the graph estimates with ones based on the “test” dataset. A useful measurement is the “number of reproduced edges”, as the count of same edges from the two times of graph estimation using each method. The numbers for the low tree-rank model, lasso, horseshoe and elastic net models are 30, 12, 26 and 18, respectively. We plot these reproduced edges in Figure 7. The low tree-rank model finds many connections that are symmetric and mostly in the frontal lobe. The frontal lobe known as a “provincial hubs” (V. Farahani et al., 2021), as an important region that is known to have many connections (GeethaRamani and Sivaselvi, 2014).

7 Discussion

A tree-rank prior distribution is introduced to induce both near-connectivity and high sparsity on the network Granger causal network of a vector autoregression model, propose a fast algorithm for calculating the posterior distribution of the model parameters and also establish posterior consistency of their estimates. There are several interesting extensions to pursue in future work. The focus of this paper was one connected but highly sparse Granger causal network; nevertheless, there may be networks with relatively low tree-rank, but containing several small dense sub-networks. To accommodate this structure, we can adopt the approach in Basu et al. (2019) and consider a more flexible “low tree-rank plus sparse” structure. On the theory front, we establish the consistency of parameter estimates; it is of interest to quantify the convergence rate, even though characterizing the tree-covering probability presents an significant technical challenge. Finally, considering a union of spanning trees has potential uses in cluster analysis, a topic worth exploring.

References

Armagan, A., D. B. Dunson, and J. Lee (2013). Generalized Double Pareto Shrinkage. *Statistica Sinica* 23(1), 119.

Banbura, M., D. Giannone, and L. Reichlin (2010). Large Bayesian Vector Auto Regressions. *Journal of Applied Econometrics* 25(1), 71–92.

Basu, S. and G. Michailidis (2015). Regularized Estimation in Sparse High-Dimensional Time Series Models. *The Annals of Statistics* 43(4), 1535–1567.

Basu, S., A. Shojaie, and G. Michailidis (2015). Network Granger Causality with Inherent Grouping Structure. *The Journal of Machine Learning Research* 16(1), 417–453.

Basu, S., L. Xiangqi, and G. Michailidis (2019). Low Rank and Structured Modeling of High-Dimensional Vector Autoregressions. *IEEE Transactions on Signal Processing* 67(5), 1207–1222.

Carvalho, C. M., N. G. Polson, and J. G. Scott (2010). The Horseshoe Estimator for Sparse Signals. *Biometrika* 97(2), 465–480.

Cattell, R. B. (1966). The Scree Test for the Number of Factors. *Multivariate Behavioral Research* 1(2), 245–276.

Cobb, A. D. and B. Jalaian (2021). Scaling Hamiltonian Monte Carlo Inference for Bayesian Neural Networks with Symmetric Splitting. *Uncertainty in Artificial Intelligence*.

Desikan, R. S., F. Ségonne, B. Fischl, B. T. Quinn, B. C. Dickerson, D. Blacker, R. L. Buckner, A. M. Dale, R. P. Maguire, and B. T. Hyman (2006). An Automated Labeling System for Subdividing the Human Cerebral Cortex on MRI Scans Into Gyral Based Regions of Interest. *Neuroimage* 31(3), 968–980.

Eichler, M. (2007). Granger Causality and Path Diagrams for Multivariate Time Series. *Journal of Econometrics* 137(2), 334–353.

Gabow, H. N. and H. H. Westermann (1992). Forests, Frames, and Games: Algorithms for Matroid Sums and Applications. *Algorithmica* 7(1), 465–497.

GeethaRamani, R. and K. Sivaselvi (2014). Human Brain Hubs (Provincial And Connector) Identification Using Centrality Measures. In *2014 International Conference on Recent Trends in Information Technology*, pp. 1–6.

Gelman, A., J. B. Carlin, H. S. Stern, D. B. Dunson, A. Vehtari, and D. B. Rubin (2013). *Bayesian Data Analysis*. CRC press.

Ghosh, S., K. Khare, and G. Michailidis (2019). High-Dimensional Posterior Consistency in Bayesian Vector Autoregressive Models. *Journal of the American Statistical Association* 114(526), 735–748.

Granger, C. (1969). Investigating Causal Relations by Econometric Models and Cross-Spectral Methods. *Econometrica* 37(3), 423–438.

Hoffman, M. D. and A. Gelman (2014). The No-U-Turn Sampler: Adaptively Setting Path Lengths in Hamiltonian Monte Carlo. *The Journal of Machine Learning Research* 15(47), 1593–1623.

Hsu, N.-J., H.-L. Hung, and Y.-M. Chang (2008). Subset Selection for Vector Autoregressive Processes Using Lasso. *Computational Statistics and Data Analysis* 52, 3645–3657.

Kock, A. B. and L. Callot (2015). Oracle Inequalities for High Dimensional Vector Autoregressions. *Journal of Econometrics* 186(2), 325–344.

Korobilis, D. (2013). VAR Forecasting Using Bayesian Variable Selection. *Journal of Applied Econometrics* 28(2), 204–230.

Li, H. and D. Pati (2017). Variable Selection Using Shrinkage Priors. *Computational Statistics & Data Analysis* 107, 107–119.

Lin, J. and G. Michailidis (2017). Regularized Estimation and Testing for High-Dimensional Multi-Block Vector-Autoregressive Models. *The Journal of Machine Learning Research* 18.

Lin, J. and G. Michailidis (2020). Regularized Estimation of High-Dimensional Factor-Augmented Vector Autoregressive (FAVAR) Models. *The Journal of Machine Learning Research* 21(117).

Loh, P.-L. and M. J. Wainwright (2012). High-Dimensional Regression With Noisy and Missing Data: Provable Guarantees With Nonconvexity. *The Annals of Statistics* 40(3), 1637–1664.

Lütkepohl, H. (2005). *New Introduction to Multiple Time Series Analysis*. Springer Science & Business Media.

Maziarz, M. (2015). A Review of the Granger-Causality Fallacy. *The Journal of Philosophical Economics* 8(2), 86–105.

Michailidis, G. and F. d'Alché Buc (2013). Autoregressive Models for Gene Regulatory Network Inference: Sparsity, Stability and Causality Issues. *Mathematical Biosciences* 246(2), 326–334.

Murota, K. (1998). Discrete Convex Analysis. *Mathematical Programming* 83(1-3), 313–371.

Nash-Williams, C. S. J. (1964). Decomposition of Finite Graphs into Forests. *Journal of the London Mathematical Society* 1(1), 12–12.

Neal, R. M. (2010). *MCMC Using Hamiltonian Dynamics*. Chapman and Hall—CRC Press.

Nicholson, W. B., I. Wilms, J. Bien, and D. S. Matteson (2020). High Dimensional Forecasting via Interpretable Vector Autoregression. *The Journal of Machine Learning Research* 21, 1–52.

Paszke, A., S. Gross, S. Chintala, G. Chanan, E. Yang, Z. DeVito, Z. Lin, A. Desmaison, L. Antiga, and A. Lerer (2017). Automatic Differentiation in PyTorch.

Polson, N. G. and J. G. Scott (2010). Shrink Globally, Act Locally: Sparse Bayesian Regularization and Prediction. *Bayesian Statistics* 9(501-538), 105.

Prim, R. C. (1957). Shortest Connection Networks and Some Generalizations. *The Bell System Technical Journal* 36(6), 1389–1401.

Schwaller, L., S. Robin, and M. Stumpf (2019). Closed-Form Bayesian Inference of Graphical Model Structures by Averaging Over Trees. *Journal de la Société Française de Statistique* 160(2), 1–23.

Seth, A. K., A. B. Barrett, and L. Barnett (2015). Granger Causality Analysis in Neuroscience and Neuroimaging. *Journal of Neuroscience* 35(8), 3293–3297.

Sims, C. A. (1989). A Nine Variable Probabilistic Macroeconomic Forecasting Model. *National Bureau of Economic Research*, 179–212.

Stock, J. H. and M. W. Watson (2016). Dynamic Factor Models, Factor-Augmented Vector Autoregressions, and Structural Vector Autoregressions in Macroeconomics. In *Handbook of Macroeconomics*, Volume 2, pp. 415–525. Elsevier.

V. Farahani, F., M. Fafrowicz, W. Karwowski, B. Bohaterewicz, A. M. Sobczak, A. Ceglarek, A. Zyrkowska, M. Ostrogorska, B. Sikora-Wachowicz, K. Lewandowska, H. Oginska,

A. Beres, M. Hubalewska-Mazgaj, and T. Marek (2021). Identifying Diurnal Variability of Brain Connectivity Patterns Using Graph Theory. *Brain Sciences* 11(1).

Appendix

A Proofs

A.1 Proof for Theorem 1

The lower bound is trivial. For the upper bound, note that $\bar{G} \subseteq F$, with F a complete graph $F = \{V, E_F\}$, with E_F containing all possible pairs of undirected (i, j) . Then consider the tree \tilde{T}^l with edge sets $E_{\tilde{T}^l} = \{([l+1]_p, 1), ([l+2]_p, 2), \dots, ([l+p-1]_p, p-1)\}$, where $[l+i]_p = l+i$ if $l+i \leq p$, otherwise $[l+i]_p = l+i-p$ — that is, $E_{\tilde{T}^l}$ corresponds to the l -diagonal elements (the diagonal with l row offset from the main diagonal) in a $p \times p$ matrix.

Therefore, we can see that $\cup_{l=1}^{p-1} \tilde{T}^l$ includes all the edges in F , therefore, the tree rank of F is at most $p-1$, hence so is for \bar{G} .

A.2 Proof for Theorem 3

For a complex matrix $A \in \mathbb{C}^{p \times p}$, A^* denotes the conjugate transpose of A . We use \bar{z} to denote the complex conjugate of a complex number z . The modulus of z is denoted by $|z|$. For a complex matrix $A \in \mathbb{C}^{p \times p}$, A_H denotes the Hermitian part of A : $A_H = 2^{-1}(A + A^*)$. Let $A(C, z) := C^{(1)}z + \dots + C^{(d)}z^d$. We use $B(z) = 2^{-1}[A(C, z) + A^*(C, z)]$ to denote its Hermitian part. Since $B(z)$ is Hermitian, we define the Laplacian as $L_B(z) := D_B(z) - B(z)$ with $D_B(z) = \text{diag}\{\sum_{j=1}^p |B(z)_{ij}|\}_i$. Clearly $L_B(z)$ is Hermitian hence all eigenvalues of $L_B(z)$ are real, denoted by $\lambda_1 \leq \lambda_2 \leq \dots \leq \lambda_p$.

For ease of notation, we omit $._B(z)$ for now. For any $w = (w_1, \dots, w_p)^T \in \mathbb{C}^p$, we have

$$\begin{aligned}
w^* L w &= w^* (D - B) w \\
&= \sum_{i=1}^p \bar{w}_i \left(\sum_{j=1}^p |B_{ij}| \right) w_i - \sum_{i < j} \bar{w}_i B_{ij} w_j - \sum_{j < i} \bar{w}_i B_{ij} w_j - \sum_{i=1}^n \bar{w}_i B_{ii} w_i \\
&\stackrel{(a)}{=} \sum_{i=1}^p |w_i|^2 \left(\sum_{j \neq i} |B_{ij}| \right) - 2 \sum_{i < j} \bar{w}_i B_{ij} w_j \\
&= \frac{1}{2} \sum_{i=1}^p \sum_{j \neq i} |B_{ij}| \left(\bar{w}_i - \frac{\bar{B}_{ij}}{|B_{ij}|} \bar{w}_j \right) \left(w_i - \frac{B_{ij}}{|B_{ij}|} w_j \right) \\
&= \frac{1}{2} \sum_{i=1}^p \sum_{j \neq i} |B_{ij}| |w_i - \frac{B_{ij}}{|B_{ij}|} w_j|^2 \\
&\geq 0.
\end{aligned} \tag{15}$$

where (a) is due to $B_{i,j} = \bar{B}_{j,i}$ and $|B_{i,i}| = B_{i,i}$.

Therefore, L is positive semi-definite; and it is not hard to see that $L + \varepsilon I_p$ is strictly positive definite, for any $\varepsilon > 0$.

For the complex matrix $W = I_p - A(C, z)$ to be positive definite, the sufficient and necessary condition is that its Hermitian part is positive definite. That is:

$$\begin{aligned}
W_H &= I_p - B \\
&= (L + \varepsilon I_p) + (1 - \varepsilon) I_p - D_B
\end{aligned} \tag{16}$$

should be positive definite. Since D_B is diagonal, therefore, a sufficient condition is to have:

$$1 - \varepsilon - (D_B)_{ii} \geq 0 \tag{17}$$

for all $i = 1, \dots, p$. This is equivalent to

$$\sum_{j=1}^p \left| \frac{1}{2} [A(C, z) + A(C, z)^*]_{ij} \right| \leq 1 - \varepsilon, \tag{18}$$

or

$$\sum_{j=1}^p |C_{i,j}^{(1)} z + \dots + C_{i,j}^{(d)} z^d + C_{j,i}^{(1)} \bar{z} + \dots + C_{j,i}^{(d)} \bar{z}^d| \leq 2 - 2\varepsilon, \tag{19}$$

Taking $\varepsilon \rightarrow 0_+$, we have a sufficient condition for stability:

$$\sum_{j=1}^p |C_{i,j}^{(1)}z + \dots + C_{i,j}^{(d)}z^d + C_{j,i}^{(1)}\bar{z} + \dots + C_{j,i}^{(d)}\bar{z}^d| < 2 \quad \forall z \in \mathbb{C} : |z| \leq 1 \quad (20)$$

for all $i = 1, \dots, p$.

Using the polar coordinate for $z = r \exp(\mathbb{I}x)$, where $r \in [0, 1]$ and \mathbb{I} is the imaginary unit.

The above becomes:

$$\sum_{j=1}^p \left| \sum_{k=1}^d [C_{i,j}^{(k)} r^k \exp(\mathbb{I}kx) + C_{j,i}^{(k)} r^k \exp(-\mathbb{I}kx)] \right| < 2 \quad \forall z \in \mathbb{C} : |z| \leq 1 \quad (21)$$

For each term on the left hand side, it has

$$\begin{aligned} & \left| \sum_{k=1}^d [(C_{i,j}^{(k)} + C_{j,i}^{(k)}) \cos(kx)r^k + \mathbb{I}(C_{i,j}^{(k)} - C_{j,i}^{(k)}) \sin(kx)r^k] \right| \\ &= \left\{ \left[\sum_{k=1}^d (C_{i,j}^{(k)} + C_{j,i}^{(k)}) \cos(kx)r^k \right]^2 + \left[\sum_{k=1}^d (C_{i,j}^{(k)} - C_{j,i}^{(k)}) \sin(kx)r^k \right]^2 \right\}^{1/2} \\ &\stackrel{(a)}{\leq} \left\{ \sum_{k=1}^d (C_{i,j}^{(k)} + C_{j,i}^{(k)})^2 r^{2k} \sum_{k=1}^d \cos^2(kx) + \sum_{k=1}^d (C_{i,j}^{(k)} - C_{j,i}^{(k)})^2 r^{2k} \sum_{k=1}^d \sin^2(kx) \right\}^{1/2} \\ &= \left\{ \left[\sum_{k=1}^d \cos^2(kx) + \sum_{k=1}^d \sin^2(kx) \right] \sum_{k=1}^d [(C_{i,j}^{(k)})^2 + (C_{j,i}^{(k)})^2] r^{2k} \right. \\ &\quad \left. + \left[\sum_{k=1}^d \cos^2(kx) - \sum_{k=1}^d \sin^2(kx) \right] \sum_{k=1}^d [2(C_{i,j}^{(k)})(C_{j,i}^{(k)})] r^{2k} \right\}^{1/2} \\ &= \left\{ d \sum_{k=1}^d [(C_{i,j}^{(k)})^2 + (C_{j,i}^{(k)})^2] r^{2k} + 2 \left[\sum_{k=1}^d \cos(2kx) \right] \sum_{k=1}^d C_{i,j}^{(k)} C_{j,i}^{(k)} r^{2k} \right\}^{1/2} \end{aligned} \quad (22)$$

where (a) uses the Cauchy-Schwarz inequality, we denote:

$$\begin{aligned} g_x &= \frac{1}{d} \sum_{k=1}^d \cos(2kx) \\ &= \frac{1}{2d} [1 + 2 \sum_{k=1}^d \cos(2kx)] - \frac{1}{2d} \\ &= \frac{2\pi}{2d} D_d(2x) - \frac{1}{2d}, \end{aligned} \quad (23)$$

where $D_d(x)$ denotes the Dirichlet kernel, which has the maximum of $(2d+1)/(2\pi)$, and the minimum around $-c_0(2d+1)/(2\pi)$ for $d \geq 10$, with $c_0 \approx 0.2172$. Taking $c_1 = 0.22$, we have $D_d(x) > -0.22(2d+1)/(2\pi)$. Slightly adjusting the constant, we have:

$$-0.4 - \frac{0.61}{d} < g(x) \leq 1 \quad (24)$$

for all $d \in \mathbb{Z}_+$, we denote $g_0 = -0.4 - 0.61/d$.

Continuing on the inequality,

$$\begin{aligned} & \left\{ d \sum_{k=1}^d [(C_{i,j}^{(k)})^2 + (C_{j,i}^{(k)})^2] r^{2k} + dg_x \left[\sum_{k=1}^d 2C_{i,j}^{(k)} C_{j,i}^{(k)} \right] r^{2k} \right\}^{1/2} \\ &= \left\{ d \sum_{k=1}^d \left([C_{i,j}^{(k)} + g_x C_{j,i}^{(k)}]^2 + (1 - g_x^2)(C_{j,i}^{(k)})^2 \right) r^{2k} \right\}^{1/2} \\ &\stackrel{(a)}{\leq} \left\{ d \sum_{k=1}^d \left([C_{i,j}^{(k)} + g_x C_{j,i}^{(k)}]^2 + (1 - g_x^2)(C_{j,i}^{(k)})^2 \right) \right\}^{1/2} \end{aligned} \quad (25)$$

where (a) is due to each term is non-negative, hence $r^2 = 1$ maximizes the right hand side. It is not hard to see that, to maximize the right hand side, if $\sum_{k=1}^d C_{i,j}^{(k)} C_{j,i}^{(k)} \geq 0$, we take $g_x = 1$; otherwise, we take $g_x = \min_x g_x$. Further with $g_0 \leq \min_x g_x$, we have $g_0 \sum_{k=1}^d C_{i,j}^{(k)} C_{j,i}^{(k)} \geq \min_x g_x \sum_{k=1}^d C_{i,j}^{(k)} C_{j,i}^{(k)}$ when $\sum_{k=1}^d C_{i,j}^{(k)} C_{j,i}^{(k)} < 0$.

Therefore, we have the right hand side:

$$\begin{aligned} & \left\{ d \sum_{k=1}^d \left([C_{i,j}^{(k)} + g_x C_{j,i}^{(k)}]^2 + (1 - g_x^2)(C_{j,i}^{(k)})^2 \right) \right\}^{1/2} \\ &\leq \sqrt{d} \left\{ \max_{h \in \{1, g_0\}} \left(\sum_{k=1}^d \left([C_{i,j}^{(k)} + h C_{j,i}^{(k)}]^2 + (1 - h^2)(C_{j,i}^{(k)})^2 \right) \right)^{1/2} \right\}^{1/2}. \end{aligned} \quad (26)$$

Therefore, we have

$$\begin{aligned}
& \sum_{j=1}^p \left| \sum_{k=1}^d [C_{i,j}^{(k)} r^k \exp(\mathbb{I}kx) + C_{j,i}^{(k)} r^k \exp(-\mathbb{I}kx)] \right| \\
& \leq \sup_{g_x \in [\min_x g_x, 1]} \sum_{j=1}^p \left\{ d \sum_{k=1}^d \left([C_{i,j}^{(k)} + g_x C_{j,i}^{(k)}]^2 + (1 - g_x^2)(C_{j,i}^{(k)})^2 \right) \right\}^{1/2} \\
& \stackrel{(a)}{\leq} \sqrt{d} \sum_{j=1}^p \max_{h_j \in \{g_0, 1\}} \left\{ \sum_{k=1}^d \left([C_{i,j}^{(k)} + h_j C_{j,i}^{(k)}]^2 + (1 - h_j^2)(C_{j,i}^{(k)})^2 \right) \right\}^{1/2},
\end{aligned} \tag{27}$$

where (a) is due to the supremum of a sum over $g_x \in [\min_x g_x, 1]$ is smaller or equal to the sum of the supremum of each term, and each supremum is smaller than the one replacing g_x by $h_j \in \{g_0, 1\}$.

A.3 Proof for Theorem 4

First we note that

$$\mathbb{P}_0\{||c - c_0|| > \eta \mid \Phi, y, X\} \leq \mathbb{P}_0\{||c - \hat{c}|| > \eta/2 \mid \Phi, y, X\} + \mathbb{P}_0\{||\hat{c} - c_0|| > \eta/2 \mid \Phi, y, X\},$$

where $\hat{c} = \{\hat{\Gamma} + \Phi^{-1}/N\}^{-1}\hat{\gamma}$.

Let $\Sigma_\varepsilon^{-1} = Q_\Sigma^T Q_\Sigma$ be the symmetric decomposition, the Woodbury identity gives:

$$\begin{aligned}
(\Sigma_\varepsilon^{-1} \otimes X^T X + \Phi^{-1})^{-1} &= \{(Q_\Sigma^T \otimes X^T)(Q_\Sigma \otimes X) + \Phi^{-1}\}^{-1} \\
&= \Phi - \Phi(Q_\Sigma^T \otimes X^T)\{I + (Q_\Sigma \otimes X)\Phi(Q_\Sigma^T \otimes X^T)\}^{-1}(Q_\Sigma^T \otimes X^T)\Phi.
\end{aligned}$$

Therefore, if $(i, j) \notin \bigcup_{l=1}^m T^l$, then with $\sum_{l=1}^m s_l A_{i,j}^l \rightarrow 0$ uniformly, we have $(c_{i,j,k} \mid \Sigma_\varepsilon, r, \eta, s, A)$ converge to a point mass at zero. On the other hand, for those $(i, j) \in \bigcup_{l=1}^m T^l$, due to the lower-boundedness as described in A3, we know $\Phi_{i,j,k}^{-1} < \kappa$ for some constant $\kappa > 0$. Moreover, by Assumption A2, for those $(i, j) \notin \bigcup_{l=1}^m T^l$, we have $\Phi_{i,j,k}^{-1} < \kappa/\epsilon^2$, where ϵ is defined in A2. Therefore, for any fixed $\epsilon > 0$, $\|\Phi^{-1}\|$ is bounded.

(i) Bound the distance between \hat{c} and c_0 given Φ :

$$\begin{aligned}
\hat{c} - c_0 &= [\hat{\Gamma} + \Phi^{-1}/N]^{-1} \hat{\gamma} - c_0 \\
&= [\hat{\Gamma} + \Phi^{-1}/N]^{-1} (\hat{\gamma} - \hat{\Gamma}c_0 + \hat{\Gamma}c_0) - c_0 \\
&= [\hat{\Gamma} + \Phi^{-1}/N]^{-1} (\hat{\gamma} - \hat{\Gamma}c_0) + [\hat{\Gamma} + \Phi^{-1}/N]^{-1} (\hat{\Gamma} + \Phi^{-1}/N - \Phi^{-1}/N)c_0 - c_0 \\
&= [\hat{\Gamma} + \Phi^{-1}/N]^{-1} (\hat{\gamma} - \hat{\Gamma}c_0 - \Phi^{-1}/Nc_0).
\end{aligned} \tag{28}$$

Hence,

$$\begin{aligned}
&||\hat{c} - c_0|| \\
&= ||[\hat{\Gamma} + \Phi^{-1}/N]^{-1} (\hat{\gamma} - \hat{\Gamma}c_0 - \Phi^{-1}/Nc_0)|| \\
&\leq ||[\hat{\Gamma} + \Phi^{-1}/N]^{-1}|| \cdot \{ ||\Phi^{-1}/Nc_0|| + ||\hat{\gamma} - \hat{\Gamma}c_0|| \}.
\end{aligned} \tag{29}$$

Note that,

$$\begin{aligned}
&||[\hat{\Gamma} + \Phi^{-1}/N]^{-1}|| = \lambda_{\max}[\hat{\Gamma} + \Phi^{-1}/N]^{-1} = 1/\lambda_{\min}[\hat{\Gamma} + \Phi^{-1}/N] \\
&\stackrel{(a)}{\leq} 1/\{\lambda_{\min}(\hat{\Gamma}) + \lambda_{\min}\{\Phi^{-1}/N\}\} \leq 1/\lambda_{\min}(\hat{\Gamma}),
\end{aligned} \tag{30}$$

where (a) is due to the positive definiteness of Φ^{-1} and $\hat{\Gamma}$. Together with $\lambda_{\min}(\hat{\Gamma}) = 1/||(\Sigma_{\varepsilon}^{-1} \otimes X'X/N)^{-1}|| = 1/(||\Sigma_{\varepsilon}|| \cdot ||(X'X/N)^{-1}||)$, we have $||[\hat{\Gamma} + \Phi^{-1}/N]^{-1}|| \leq ||\Sigma_{\varepsilon}||/\lambda_{\min}(X'X/N)$.

Thus, together with (29), we have

$$\begin{aligned}
&\mathbb{P}_0(||\hat{c} - c_0|| > \eta \mid \Phi, y, X) \\
&\leq \mathbb{P}_0(||[\hat{\Gamma} + \Phi^{-1}/N]^{-1}|| \cdot \{ ||\Phi^{-1}/Nc_0|| + ||\hat{\gamma} - \hat{\Gamma}c_0|| \} > \eta \mid \Phi, y, X) \\
&\stackrel{(a)}{\leq} \mathbb{P}_0(||\Sigma_{\varepsilon}||/\lambda_{\min}(X'X/N) \cdot (||\Phi^{-1}/Nc_0|| + ||\hat{\gamma} - \hat{\Gamma}c_0||) > \eta \mid \Phi, y, X) \\
&\leq \mathbb{P}_0(\lambda_{\min}(X'X/N) < \lambda_1 \mid y, X) + \mathbb{P}_0(||\Phi^{-1}/Nc_0|| + ||\hat{\gamma} - \hat{\Gamma}c_0|| > \eta\lambda_1/||\Sigma_{\varepsilon}|| \mid \Phi, y, X) \\
&\leq \mathbb{P}_0(\lambda_{\min}(X'X/N) < \lambda_1 \mid y, X) + \mathbb{P}_0(||\Phi^{-1}/Nc_0|| > \eta\lambda_1/(2||\Sigma_{\varepsilon}||) \mid \Phi, y, X) \\
&\quad + \mathbb{P}_0(||\hat{\gamma} - \hat{\Gamma}c_0|| > \eta\lambda_1/(2||\Sigma_{\varepsilon}||) \mid \Phi, y, X),
\end{aligned} \tag{31}$$

where (a) is due to $\|[\hat{\Gamma} + \Phi^{-1}/N]^{-1}\| \leq \|\Sigma_\varepsilon\|/\lambda_{\min}(X'X/N)$ and λ_1 is defined in Proposition B.2 in Ghosh et al. (2019). Assumption A3 guarantees the validity of Proposition B.2 in Ghosh et al. (2019), hence the first term on the right hand side of (31) is less than $2 \exp\{-\sqrt{Np}\}$.

By Assumption A2, for those $(i, j) \in \bigcup_{l=1}^m T^l$, due to the lower-boundedness as described in A3, we know $\Phi_{i,j,k}^{-1} < \kappa$ for some constant $\kappa > 0$. Moreover, for those $(i, j) \notin \bigcup_{l=1}^m T^l$, we have $\Phi_{i,j,k}^{-1} < \kappa/\epsilon^2$, where ϵ is defined in A2. Therefore, for any fixed $\epsilon > 0$, $\|\Phi^{-1}\|$ is bounded. Together with Assumption A4 $\|c_0\| \leq K$, we have

$$\|\Phi^{-1}c_0\| = o(N), \quad (32)$$

which ensures the second term on the right hand side of (31) converges to 0 as $N \rightarrow \infty$.

Note that $\|\hat{\gamma} - \hat{\Gamma}c_0\| = \|\text{vec}(X^T E/N)\| = \|X^T E/N\|_F \leq \sqrt{dp}\|X^T E/N\|$. By Assumption A1, we have $\|\hat{\gamma} - \hat{\Gamma}c_0\| \leq \mathbb{Q}(c_0, \Sigma_\varepsilon)\sqrt{dp^2/N}$. Therefore, for sufficiently large N , we have $\|\hat{\gamma} - \hat{\Gamma}c_0\| \leq \eta\lambda_1/(2\|\Sigma_\varepsilon\|)$, which implies $\mathbb{P}_0(\|\hat{\gamma} - \hat{\Gamma}c_0\| > \eta\lambda_1/(2\|\Sigma_\varepsilon\|) \mid y, X) = 0$. Combining the results above gives

$$\mathbb{P}_0(\|\hat{c} - c_0\| > \eta \mid \Phi, y, X) \rightarrow 0, \text{ as } N \rightarrow \infty. \quad (33)$$

(ii) Bound the distance between \hat{c} and c given Φ :

Recall that $c \mid \Phi, y, X \sim \text{No}(\hat{c}, [\hat{\Gamma} + \Phi^{-1}/N]^{-1}/N)$ and define $\tilde{\Sigma}_\varepsilon$ as $[\hat{\Gamma} + \Phi^{-1}/N]^{-1}/N$. First note that $Z := \tilde{\Sigma}_\varepsilon^{-1/2}(c - \hat{c}) \mid \Phi, y, X \sim \text{No}(\vec{0}, I_{dp^2})$.

Also,

$$\begin{aligned} \|c - \hat{c}\| &= \|\tilde{\Sigma}_\varepsilon^{1/2} \cdot \tilde{\Sigma}_\varepsilon^{-1/2}(c - \hat{c})\| \\ &= \|\tilde{\Sigma}_\varepsilon^{1/2}Z\| \\ &\leq \|\tilde{\Sigma}_\varepsilon^{1/2}\| \cdot \|Z\| \\ &= (N\|\tilde{\Sigma}_\varepsilon\|)^{1/2} \cdot \|Z/\sqrt{N}\|. \end{aligned} \quad (34)$$

As previously stated, we have,

$$N\|\tilde{\Sigma}_\varepsilon\| = \|[\hat{\Gamma} + \Phi^{-1}/N]^{-1}\| \leq \|\Sigma_\varepsilon\|/\lambda_{\min}(X'X/N). \quad (35)$$

Therefore,

$$\|c - \hat{c}\| \leq \{\|\Sigma_\varepsilon\|/\lambda_{\min}(X'X/N)\}^{1/2} \cdot \|Z/\sqrt{N}\|. \quad (36)$$

Hence,

$$\begin{aligned} & \mathbb{P}_0(\|c - \hat{c}\| > \eta \mid \Phi, y, X) \\ & \leq \mathbb{P}_0(\{\|\Sigma_\varepsilon\|/\lambda_{\min}(X'X/N)\}^{1/2} \cdot \|Z/\sqrt{N}\| > \eta \mid \Phi, y, X) \\ & \leq \mathbb{P}_0(\lambda_{\min}(X'X/N) < \lambda_1) + \mathbb{P}_0(\|\Sigma_\varepsilon\|^{1/2} \|Z/\sqrt{N}\| > \eta(\lambda_1)^{1/2} \mid \Phi, y, X) \quad (37) \\ & = \mathbb{P}_0(\lambda_{\min}(X'X/N) < \lambda_1) + \mathbb{P}_0(\|Z/\sqrt{N}\| > \eta(\lambda_1/\|\Sigma_\varepsilon\|)^{1/2} \mid \Phi, y, X) \\ & = \mathbb{P}_0(\lambda_{\min}(X'X/N) < \lambda_1) + \mathbb{P}_0(\|Z\|^2 > N\eta^2\lambda_1/\|\Sigma_\varepsilon\| \mid \Phi, y, X). \end{aligned}$$

By Proposition B.2 in Ghosh et al. (2019), the first term on the right hand side of (37) converges to 0 as $N \rightarrow \infty$.

Next, we show $\mathbb{P}_0(\|Z\|^2 > N\eta^2\lambda_1/\|\Sigma_\varepsilon\| \mid \Phi, y, X) \rightarrow 0$, as $N \rightarrow \infty$. Note that $\|Z\|^2 \sim \chi_2(dp^2)$, which implies $\mathbb{E}_0(\|Z\|^2) = dp^2$, $\mathbb{V}_0(\|Z\|^2) = 2dp^2$. Using Chebyshev's inequality gives

$$\begin{aligned} & \mathbb{P}_0\{\|Z\|^2 - dp^2 > N\eta^2\lambda_1/\|\Sigma_\varepsilon\| \mid \Phi, y, X\} < 2dp^2/(N\eta^2\lambda_1/\|\Sigma_\varepsilon\|)^2 \\ & = 2(p/N)^2 \cdot d\|\Sigma_\varepsilon\|^2/(\eta^2\lambda_1). \end{aligned} \quad (38)$$

Thus,

$$\begin{aligned} & \mathbb{P}_0(\|Z\|^2 > N\eta^2\lambda_1/\|\Sigma_\varepsilon\| \mid \Phi, y, X) \\ & \leq \mathbb{P}_0(\|Z\|^2 - dp^2 > N\eta^2\lambda_1/\|\Sigma_\varepsilon\| \mid \Phi, y, X) + \mathbb{P}_0(dp^2 > N\eta^2\lambda_1/\|\Sigma_\varepsilon\| \mid \Phi, y, X). \end{aligned} \quad (39)$$

Combining the two sections above, we have

$$\mathbb{P}_0\{||c - c_0|| > \eta \mid \Phi, y, X\} \rightarrow 0, \text{ as } N \rightarrow \infty.$$

(iii) Show convergence of posterior probability

First note that $c \mid \Phi, y, X \sim \text{No}(\hat{c}, \frac{1}{N}(\hat{\Gamma} + \frac{\Phi^{-1}}{N})^{-1})$.

We obtain the marginal posterior distribution of $(\Phi \mid y, X)$ by integrating out the regression coefficient c :

$$\begin{aligned} \mathbb{P}_0(\Phi \mid y, X) &\propto \int \mathcal{L}(c, \Phi; y) \pi_0(c \mid \Phi) \pi_0(\Phi) \, dc \\ &\propto \int \exp\left\{-\frac{1}{2}\{y - (I_p \otimes X)c\}^T (\Sigma_\varepsilon^{-1} \otimes I_{T-d})\{y - (I_p \otimes X)c\}\right\} \exp\left\{-\frac{1}{2}c^T \Phi^{-1} c\right\} \{\det(\Phi)\}^{-1/2} \pi_0(\Phi) \, dc \\ &\propto \{\det(\hat{\Gamma} + \Phi^{-1}/N)\}^{-1/2} \pi_0(\Phi) \{\det(\Phi)\}^{-1/2} \exp\{N\hat{\gamma}^T [\hat{\Gamma} + \Phi^{-1}/N]^{-1}\hat{\gamma}/2\}. \end{aligned} \tag{40}$$

Comparing the posterior densities of two Φ_{**} and Φ_* :

$$\begin{aligned} \frac{\mathbb{P}_0(\Phi_{**} \mid y, X)}{\mathbb{P}_0(\Phi_* \mid y, X)} &= \frac{\det^{-1/2}[\hat{\Gamma} + \Phi_{**}^{-1}/N] \det^{-1/2}(\Phi_{**}) \pi_0(\Phi_{**})}{\det^{-1/2}[\hat{\Gamma} + \Phi_*^{-1}/N] \det^{-1/2}(\Phi_*) \pi_0(\Phi_*)} \\ &\times \exp\left[N\hat{\gamma}^T \left\{[\hat{\Gamma} + \Phi_{**}^{-1}/N]^{-1} - [\hat{\Gamma} + \Phi_*^{-1}/N]^{-1}\right\} \hat{\gamma}/2\right]. \end{aligned} \tag{41}$$

By Assumption A2, we know $\Phi_{i,j,k,**}^{-1} \leq \min\{\kappa, \kappa/\epsilon^2\}$. Since Φ_{**}^{-1} is diagonal, this guarantees the boundedness of $\det\{\Phi_{**}^{-1}\}$. Similarly, $\det\{\Phi_*^{-1}\}$ is bounded.

Next, we show $\det\{\hat{\Gamma} + \Phi_{**}^{-1}/N\}$ is bounded for sufficiently large N . Then together with $\det^{\frac{1}{2}}(\Gamma + \Phi_*^{-1}/N)$ is greater than 0, we obtain the boundedness of $\det^{\frac{1}{2}}(\Gamma + \Phi_{**}^{-1}/N)$ and $\det^{\frac{1}{2}}(\Gamma + \Phi_*^{-1}/N)$ for sufficiently large N .

By Assumption A3 $0 < \sup_{N \geq 1} \lambda_{\max}(\Gamma_y(0)) < \infty$ and Proposition B.2 in Ghosh et al. (2019), there exists $0 < \lambda_2 < \infty$, such that $\mathbb{P}_0\{\lambda_{\max}(X'X/N) > \lambda_2\} \leq 2 \exp\{-2\sqrt{Np}\}$. This ensures that $\lambda_{\max}(X'X/N) < \lambda_2$ with probability at least $1 - 2 \exp\{-2\sqrt{Np}\}$. Also note that

$\det\{\hat{\Gamma} + \Phi_{**}^{-1}/N\} = \prod_{i=1}^{dp^2} \lambda_i\{\hat{\Gamma} + \Phi_{**}^{-1}/N\}$, where $\lambda_i\{\hat{\Gamma} + \Phi_{**}^{-1}/N\}$ is the i^{th} largest eigenvalue of $\hat{\Gamma} + \Phi_{**}^{-1}/N$.

$\lambda_{\max}(\hat{\Gamma} + \Phi_{**}^{-1}/N) \leq \lambda_{\max}(\hat{\Gamma}) + \lambda_{\max}(\Phi_{**}^{-1}/N)$ leads to $\det\{\hat{\Gamma} + \Phi_{**}^{-1}/N\} \leq [\lambda_{\max}(\hat{\Gamma}) + \lambda_{\max}(\Phi_{**}^{-1}/N)]^{dp^2}$. Also, $\lambda_{\max}(\hat{\Gamma}) = \|\Sigma_\varepsilon\| \lambda_{\max}(X'X/N) \leq \lambda_2 \|\Sigma_\varepsilon\|$ with probability at least $1 - 2 \exp\{-2\sqrt{Np}\}$, together with $\lambda_{\max}(\{\Phi_{**}^{-1}/N\})$ is bounded as N goes to ∞ , we have $\det\{\hat{\Gamma} + \Phi_{**}^{-1}/N\}$ is bounded with probability at least $1 - 2 \exp\{-2\sqrt{Np}\}$.

Without loss of generality, we only consider Φ_* with $\pi_0(\Phi_{**})$ is greater than 0, which guarantees the boundedness of the term $\pi_0(\Phi_{**})/\pi_0(\Phi_*)$. Combining the results above, for sufficiently large N , we have

$$\frac{\det^{-1/2}[\hat{\Gamma} + \Phi_{**}^{-1}/N] \det^{-1/2}(\Phi_{**}) \pi_0(\Phi_{**})}{\det^{-1/2}[\hat{\Gamma} + \Phi_*^{-1}/N] \det^{-1/2}(\Phi_*) \pi_0(\Phi_*)} \leq H(X, \tau), \quad (42)$$

where $H(X, \tau)$ is a bounded positive function.

Next, we focus on $\exp\{N/2\hat{\gamma}^T(\hat{\Gamma} + \Phi_{**}^{-1}/N)^{-1}\hat{\gamma} - \frac{N}{2}\hat{\gamma}^T(\hat{\Gamma} + \Phi_*^{-1}/N)^{-1}\hat{\gamma}\}$ and show it goes to 0 in probability, with fixed p and sufficiently large N .

We divide $N\hat{\gamma}^T(\hat{\Gamma} + \frac{\Phi_{**}^{-1}}{N})^{-1}\hat{\gamma}$ into three parts:

$$\begin{aligned} & N\hat{\gamma}^T[\hat{\Gamma} + \Phi_{**}^{-1}/N]^{-1}\hat{\gamma} \\ &= N(\hat{\gamma} - \hat{\Gamma}c_0 + \hat{\Gamma}c_0)^T[\hat{\Gamma} + \Phi_{**}^{-1}/N]^{-1}(\hat{\gamma} - \hat{\Gamma}c_0 + \hat{\Gamma}c_0) \\ &= N(\hat{\Gamma}c_0)^T[\hat{\Gamma} + \Phi_{**}^{-1}/N]^{-1}\hat{\Gamma}c_0 \\ &+ N(\hat{\gamma} - \hat{\Gamma}c_0)^T[\hat{\Gamma} + \Phi_{**}^{-1}/N]^{-1}(\hat{\gamma} - \hat{\Gamma}c_0) \\ &+ 2N(\hat{\Gamma}c_0)^T[\hat{\Gamma} + \Phi_{**}^{-1}/N]^{-1}(\hat{\gamma} - \hat{\Gamma}c_0). \end{aligned} \quad (43)$$

Thus,

$$\begin{aligned}
& N\hat{\gamma}^T[\hat{\Gamma} + \Phi_{\star\star}^{-1}/N]^{-1}\hat{\gamma} - N\hat{\gamma}^T[\hat{\Gamma} + \Phi_{\star}^{-1}/N]^{-1}\hat{\gamma} \\
&= \underbrace{\{N(\hat{\Gamma}c_0)^T[\hat{\Gamma} + \Phi_{\star\star}^{-1}/N]^{-1}\hat{\Gamma}c_0 - N(\hat{\Gamma}c_0)^T[\hat{\Gamma} + \Phi_{\star}^{-1}/N]^{-1}\hat{\Gamma}c_0\}}_{\mathcal{I}_1} \\
&+ \underbrace{N(\hat{\gamma} - \hat{\Gamma}c_0)^T\{[\hat{\Gamma} + \Phi_{\star\star}^{-1}/N]^{-1} - [\hat{\Gamma} + \Phi_{\star}^{-1}/N]^{-1}\}(\hat{\gamma} - \hat{\Gamma}c_0)}_{\mathcal{I}_2} \\
&+ \underbrace{2N(\hat{\Gamma}c_0)^T\{[\hat{\Gamma} + \Phi_{\star\star}^{-1}/N]^{-1} - [\hat{\Gamma} + \Phi_{\star}^{-1}/N]^{-1}\}(\hat{\gamma} - \hat{\Gamma}c_0)}_{\mathcal{I}_3}.
\end{aligned} \tag{44}$$

Next, we show \mathcal{I}_1 approaches negative infinity and $\mathcal{I}_2, \mathcal{I}_3$ are bounded for sufficiently small τ and sufficiently large N .

Consider \mathcal{I}_1 from (44),

$$\begin{aligned}
& N(\hat{\Gamma}c_0)^T[\hat{\Gamma} + \Phi_{\star\star}^{-1}/N]^{-1}\hat{\Gamma}c_0 \\
&= N(c_0)^T\hat{\Gamma}[\hat{\Gamma} + \Phi_{\star\star}^{-1}/N]^{-1}\hat{\Gamma}c_0 \\
&= N(c_0)^T(\hat{\Gamma} + \Phi_{\star\star}^{-1}/N - \Phi^{-1}/N)[\hat{\Gamma} + \Phi_{\star\star}^{-1}/N]^{-1}\hat{\Gamma}c_0 \\
&= N(c_0)^T\hat{\Gamma}c_0 - N(c_0)^T(\Phi^{-1}/N)[\hat{\Gamma} + \Phi_{\star\star}^{-1}/N]^{-1}\hat{\Gamma}c_0 \\
&= N(c_0)^T\hat{\Gamma}c_0 - N(c_0)^T(\Phi_{\star\star}^{-1}/N)[\hat{\Gamma} + \Phi_{\star\star}^{-1}/N]^{-1}(\hat{\Gamma} + \Phi_{\star\star}^{-1}/N - \Phi_{\star\star}^{-1}/N)c_0 \\
&= N(c_0)^T\hat{\Gamma}c_0 - (c_0)^T\Phi_{\star\star}^{-1}c_0 + N(c_0)^T(\Phi_{\star\star}^{-1}/N)[\hat{\Gamma} + \Phi_{\star\star}^{-1}/N]^{-1}(\Phi_{\star\star}^{-1}/N)c_0.
\end{aligned} \tag{45}$$

Thus, \mathcal{I}_1 is equivalent to

$$\begin{aligned}
& N(\hat{\Gamma}c_0)^T[\hat{\Gamma} + \Phi_{\star\star}^{-1}/N]^{-1}\hat{\Gamma}c_0 - N(\hat{\Gamma}c_0)^T[\hat{\Gamma} + \Phi_{\star}^{-1}/N]^{-1}\hat{\Gamma}c_0 \\
&= (c_0)^T\Phi_{\star\star}^{-1}c_0 - N(c_0)^T(\Phi_{\star\star}^{-1}/N)[\hat{\Gamma} + \Phi_{\star\star}^{-1}/N]^{-1}(\Phi_{\star\star}^{-1}/N)c_0 \\
&\quad - (c_0)^T\Phi_{\star}^{-1}c_0 + N(c_0)^T(\Phi_{\star}^{-1}/N)[\hat{\Gamma} + \Phi_{\star}^{-1}/N]^{-1}(\Phi_{\star}^{-1}/N)c_0.
\end{aligned} \tag{46}$$

Consider the first term on the right hand side of (46). Since $G_0 \subseteq \cup_{l=1}^m T_{\star}^l$, we have $c_{0,i,j,k} = 0$ for $(i, j) \notin \cup_{l=1}^m T_{\star}^l$. If $(i, j) \in \cup_{l=1}^m T_{\star}^l$, $\Phi_{(i,j,k)}^{-1} \leq \kappa$. This implies $(c_0)^T\Phi_{\star}^{-1}c_0 \leq \kappa\|c_0\|^2$.

Also, we show the third term on the right hand side of (46) approaches infinity as τ goes to 0. Also note that $G_0 \not\subseteq \cup_{l=1}^m T^l$. This implies that there exists some $(i, j) \notin \cup_{l=1}^m T_{**}^l$ such that $c_{0,i,j,k} > \zeta$, where ζ is a positive constant. Moreover, $\sum_{l=1}^m s_l A_{i,j}^l \rightarrow 0$ uniformly, which ensures $(c_0)^T \Phi_{**}^{-1} c_0 \rightarrow \infty$ as $\tau \rightarrow 0$. Hence, there exists $M_\tau > 0$ such that $(c_0)^T \Phi^{-1} c_0 \geq M_\tau$ and $M_\tau \rightarrow \infty$, as $\tau \rightarrow 0$.

Note that,

$$\begin{aligned}
& N(c_0)^T (\Phi_{**}^{-1}/N) [\hat{\Gamma} + \Phi_{**}^{-1}/N]^{-1} (\Phi_{**}^{-1}/N) c_0 \\
& \leq \|c_0\|^2 \|\Phi_{**}^{-1} [\hat{\Gamma} + \Phi_{**}^{-1}/N]^{-1} \Phi_{**}^{-1}\|/N \\
& \leq \|c_0\|^2 \|\Phi_{**}^{-1}\|^2 \|[\hat{\Gamma} + \Phi_{**}^{-1}/N]^{-1}\|/N \\
& \stackrel{(a)}{=} \|c_0\|^2 \|\Phi_{**}^{-1}\|_\infty^2 \|[\hat{\Gamma} + \Phi_{**}^{-1}/N]^{-1}\|/N.
\end{aligned} \tag{47}$$

where (a) is due to Φ_{**} is diagonal and positive definite, hence its largest eigenvalue is the maximal value on the diagonal.

Next, we obtain an upper bound of the second term on the right hand size of (46). Using $\|[\hat{\Gamma} + \Phi^{-1}/N]^{-1}\| \leq \|\Sigma_\varepsilon\|/\lambda_{\min}(X'X/N)$ gives

$$\begin{aligned}
& N(c_0)^T (\Phi_{**}^{-1}/N) [\hat{\Gamma} + \Phi_{**}^{-1}/N]^{-1} (\Phi_{**}^{-1}/N) c_0 \\
& \leq \|\Sigma_\varepsilon\|/\lambda_{\min}(X'X/N) \cdot \|\Phi_{**}^{-1} c_0\|^2/N \\
& \leq \|\Sigma_\varepsilon\|/\lambda_{\min}(X'X/N) \|c_0\|^2 \|\Phi_{**}^{-1}\|_\infty^2/N,
\end{aligned} \tag{48}$$

which converges to 0 as $N \rightarrow \infty$.

Similarly, for the the fourth term on the right hand size of (46),

$$N(c_0)^T (\Phi_{*}^{-1}/N) [\hat{\Gamma} + \Phi_{*}^{-1}/N]^{-1} (\Phi_{*}^{-1}/N) c_0 \leq \|\Sigma_\varepsilon\|/\lambda_{\min}(X'X/N) \|c_0\|^2 \|\Phi_{*}^{-1}\|_\infty^2/N. \tag{49}$$

Thus,

$$\mathcal{I}_1 \leq -M_\tau + \kappa \|c_0\|^2 + \|\Sigma_\varepsilon\|/\lambda_{\min}(X'X/N) \|c_0\|^2 (\|\Phi_{*}^{-1}\|_\infty^2 + \|\Phi_{**}^{-1}\|_\infty^2)/N. \tag{50}$$

Since $\|\Phi^{-1}\|_\infty \leq \min\{\kappa/\epsilon^2, \kappa\}$ and $\|\Phi_\star^{-1}\|_\infty \leq \min\{\kappa/\epsilon^2, \kappa\}$, together with (50), we have

\mathcal{I}_1 approach $-\infty$ with sufficiently small $\tau > 0$ and sufficiently large $N = N(\tau)$.

Next, we show $\mathcal{I}_2 = N(\hat{\gamma} - \hat{\Gamma}c_0)^T \{[\hat{\Gamma} + \Phi_{\star\star}^{-1}/N]^{-1} - [\hat{\Gamma} + \Phi_\star^{-1}/N]^{-1}\}(\hat{\gamma} - \hat{\Gamma}c_0)$ is bounded above.

By Assumption A1, we have $\|\hat{\gamma} - \hat{\Gamma}c_0\| \leq \mathbb{Q}(c_0, \Sigma_\varepsilon) \sqrt{dp^2/N}$. Together with $\|[\hat{\Gamma} + \Phi^{-1}/N]^{-1}\| \leq \|\Sigma_\varepsilon\|/\lambda_{\min}(X'X/N)$, we have

$$\begin{aligned} & N(\hat{\gamma} - \hat{\Gamma}c_0)^T [\hat{\Gamma} + \Phi_{\star\star}^{-1}/N]^{-1}(\hat{\gamma} - \hat{\Gamma}c_0) \\ & \leq N\|[\hat{\Gamma} + \Phi_{\star\star}^{-1}/N]^{-1}\| \cdot \|\hat{\gamma} - \hat{\Gamma}c_0\|^2 \\ & \leq \|\Sigma_\varepsilon\|/\lambda_{\min}(X'X/N) \mathbb{Q}(c_0, \Sigma_\varepsilon)^2 dp^2/N. \end{aligned} \quad (51)$$

Similarly, we obtain

$$N(\hat{\gamma} - \hat{\Gamma}c_0)^T [\hat{\Gamma} + \Phi_\star^{-1}/N]^{-1}(\hat{\gamma} - \hat{\Gamma}c_0) \leq \|\Sigma_\varepsilon\|/\lambda_{\min}(X'X/N) \mathbb{Q}(c_0, \Sigma_\varepsilon)^2 dp^2/N. \quad (52)$$

Hence,

$$\mathcal{I}_2 \leq 2\|\Sigma_\varepsilon\|/\lambda_{\min}(X'X/N) \mathbb{Q}(c_0, \Sigma_\varepsilon)^2 dp^2/N. \quad (53)$$

Finally, we show $\mathcal{I}_3 = 2N(\hat{\Gamma}c_0)^T \{[\hat{\Gamma} + \Phi_{\star\star}^{-1}/N]^{-1} - [\hat{\Gamma} + \Phi_\star^{-1}/N]^{-1}\}(\hat{\gamma} - \hat{\Gamma}c_0)$ is bounded, as $N \rightarrow \infty$.

Note that

$$\begin{aligned} & N(\hat{\Gamma}c_0)^T [\hat{\Gamma} + \Phi_{\star\star}^{-1}/N]^{-1}(\hat{\gamma} - \hat{\Gamma}c_0) \\ & = N(c_0)^T [\hat{\Gamma} + \Phi_{\star\star}^{-1}/N - \Phi_{\star\star}^{-1}/N] [\hat{\Gamma} + \Phi_{\star\star}^{-1}/N]^{-1}(\hat{\gamma} - \hat{\Gamma}c_0) \\ & = N(c_0)^T (\hat{\gamma} - \hat{\Gamma}c_0) - (c_0)^T \Phi_{\star\star}^{-1} [\hat{\Gamma} + \Phi_{\star\star}^{-1}/N]^{-1}(\hat{\gamma} - \hat{\Gamma}c_0). \end{aligned} \quad (54)$$

Similarly, we have

$$\begin{aligned} & N(\hat{\Gamma}c_0)^T [\hat{\Gamma} + \Phi_\star^{-1}/N]^{-1}(\hat{\gamma} - \hat{\Gamma}c_0) \\ & = N(c_0)^T (\hat{\gamma} - \hat{\Gamma}c_0) - (c_0)^T \Phi_\star^{-1} [\hat{\Gamma} + \Phi_\star^{-1}/N]^{-1}(\hat{\gamma} - \hat{\Gamma}c_0). \end{aligned} \quad (55)$$

Thus,

$$\mathcal{I}_3 = (c_0)^T \Phi_{\star\star}^{-1} [\hat{\Gamma} + \Phi_{\star\star}^{-1}/N]^{-1} (\hat{\gamma} - \hat{\Gamma} c_0) - (c_0)^T \Phi_{\star}^{-1} [\hat{\Gamma} + \Phi_{\star}^{-1}/N]^{-1} (\hat{\gamma} - \hat{\Gamma} c_0). \quad (56)$$

Considering the first term on the right hand side of (56), we have

$$\begin{aligned}
& |(c_0)^T \Phi_{\star\star}^{-1} [\hat{\Gamma} + \Phi_{\star\star}^{-1}/N]^{-1} (\hat{\gamma} - \hat{\Gamma} c_0)| \\
&= \left| \sum_{u_1, u_2} c_{0, u_1} [\hat{\Gamma} + \Phi_{\star\star}^{-1}/N]_{u_1, u_2}^{-1} (\hat{\gamma} - \hat{\Gamma} c_0)_{u_2} \right| \\
&\leq \sum_{u_1, u_2} |c_{0, u_1}| \cdot \left| \{\Phi_{\star\star}^{-1} (\hat{\Gamma} + \frac{\Phi_{\star\star}^{-1}}{N})^{-1}\}_{u_1, u_2} \right| \cdot |(\hat{\gamma} - \hat{\Gamma} c_0)_{u_2}| \\
&\leq \|c_0\|_{\infty} \cdot \|\hat{\gamma} - \hat{\Gamma} c_0\|_{\infty} \sum_{u_1, u_2} \left| \{\Phi_{\star\star}^{-1} [\hat{\Gamma} + \Phi_{\star\star}^{-1}/N]^{-1}\}_{u_1, u_2} \right| \\
&\leq \|c_0\|_{\infty} \cdot \|\hat{\gamma} - \hat{\Gamma} c_0\|_{\infty} \cdot dp^2 \|\Phi_{\star\star}^{-1} [\hat{\Gamma} + \Phi_{\star\star}^{-1}/N]^{-1}\|_{\infty} \\
&\leq dp^2 \|c_0\|_{\infty} \cdot \|\hat{\gamma} - \hat{\Gamma} c_0\|_{\infty} \cdot \|\Phi_{\star\star}^{-1}\|_{\infty} \|\hat{\Gamma} + \Phi_{\star\star}^{-1}/N\|^{-1} \\
&\stackrel{(a)}{\leq} dp^2 \|c_0\|_{\infty} \cdot \|\hat{\gamma} - \hat{\Gamma} c_0\| \cdot \|\Phi_{\star\star}^{-1}\|_{\infty} \|\hat{\Gamma} + \Phi_{\star\star}^{-1}/N\|^{-1} \|\hat{\Gamma} + \Phi_{\star\star}^{-1}/N\|_{\infty}, \tag{57}
\end{aligned}$$

where (a) is due to $\|\hat{\gamma} - \hat{\Gamma} c_0\|_{\infty} \leq \|\hat{\gamma} - \hat{\Gamma} c_0\|$.

Since $\|\hat{\Gamma} + \Phi_{\star\star}^{-1}/N\|^{-1} \leq \sqrt{dp^2} \|\hat{\Gamma} + \Phi_{\star\star}^{-1}/N\|^{-1}$ and $\|\hat{\Gamma} + \Phi_{\star\star}^{-1}/N\| \leq \Sigma_{\varepsilon} \|\lambda_{\min}(X'X/N)\|$,

continuing the inequality of (57), we have

$$\begin{aligned}
& |(c_0)^T \Phi_{\star\star}^{-1} [\hat{\Gamma} + \Phi_{\star\star}^{-1}/N]^{-1} (\hat{\gamma} - \hat{\Gamma} c_0)| \\
&\leq dp^2 \|c_0\|_{\infty} \cdot \|\hat{\gamma} - \hat{\Gamma} c_0\|_{\infty} \|\Phi_{\star\star}^{-1}\|_{\infty} \sqrt{dp^2} \|\hat{\Gamma} + \Phi_{\star\star}^{-1}/N\|^{-1} \\
&\leq dp^2 \|c_0\|_{\infty} \cdot \|\hat{\gamma} - \hat{\Gamma} c_0\| \cdot \|\Phi_{\star\star}^{-1}\|_{\infty} \sqrt{dp^2} \|\hat{\Gamma} + \Phi_{\star\star}^{-1}/N\|^{-1} \\
&\stackrel{(b)}{\leq} (dp^2)^{3/2} \|c_0\|_{\infty} \|\Phi_{\star\star}^{-1}\|_{\infty} \|\Sigma_{\varepsilon}\| \|\lambda_{\min}(X'X/N)\| \cdot \mathbb{Q}(c_0, \Sigma_{\varepsilon}) \sqrt{dp^2/N}, \tag{58}
\end{aligned}$$

where (b) is due to Assumption A1.

Similarly for Φ_* , the following holds,

$$\begin{aligned} & |(c_0)^T \Phi_*^{-1} [\hat{\Gamma} + \Phi_*^{-1}/N]^{-1} (\hat{\gamma} - \hat{\Gamma} c_0)| \\ & \leq (dp^2)^{3/2} \|c_0\|_\infty \|\Phi_*^{-1}\|_\infty \| \cdot \|\Sigma_\varepsilon\| / \lambda_{\min}(X'X/N) \cdot \mathbb{Q}(c_0, \Sigma_\varepsilon) \sqrt{dp^2/N}. \end{aligned} \quad (59)$$

Therefore,

$$\begin{aligned} \mathcal{I}_3 & \leq 2(dp^2)^{3/2} \|c_0\|_\infty (\|\Phi_{**}^{-1}\|_\infty + \|\Phi_*^{-1}\|_\infty) \|\Sigma_\varepsilon\| / \lambda_{\min}(X'X/N) \cdot \mathbb{Q}(c_0, \Sigma_\varepsilon) \sqrt{dp^2/N}. \end{aligned} \quad (60)$$

Combining the results about \mathcal{I}_1 , \mathcal{I}_2 and \mathcal{I}_3 , with sufficiently large $N = N(\tau)$, the following holds,

$$\begin{aligned} \mathcal{I}_1 + \mathcal{I}_2 + \mathcal{I}_3 & \leq -M_\tau + \kappa \|c_0\|^2 + \|\Sigma_\varepsilon\| / \lambda_{\min}(X'X/N) \|c_0\|^2 (\|\Phi_{**}^{-1}\|_\infty^2 + \|\Phi_*^{-1}\|_\infty^2) / N \\ & + 2\|\Sigma_\varepsilon\| / \lambda_{\min}(X'X/N) \mathbb{Q}(c_0, \Sigma_\varepsilon)^2 dp^2 / N \\ & + 2(dp^2)^{3/2} \|c_0\|_\infty (\|\Phi_{**}^{-1}\|_\infty + \|\Phi_*^{-1}\|_\infty) \|\Sigma_\varepsilon\| / \lambda_{\min}(X'X/N) \cdot \mathbb{Q}(c_0, \Sigma_\varepsilon) \sqrt{dp^2/N}. \end{aligned} \quad (61)$$

By Assumption 2, we know $\|\Phi^{-1}\|_\infty$ and $\|\Phi_*^{-1}\|_\infty$ are less than $\min\{\kappa/\epsilon^2, \kappa\}$. Note that Assumption A4 and A5 ensure the boundedness of $\|c_0\|_\infty$ and $\|\Sigma_\varepsilon\|$, respectively.

There exists sufficiently large $N_1(\tau)$, such that for $N > N_1(\tau)$,

$$\|\Sigma_\varepsilon\| \cdot \|c_0\|^2 (\|\Phi_{**}^{-1}\|_\infty^2 + \|\Phi_*^{-1}\|_\infty^2) / N \leq 1/2. \quad (62)$$

Similarly, for τ given above, there exists sufficiently large $N_2(\tau)$, such that for $N > N_2(\tau)$,

$$(dp^2)^{3/2} \|c_0\|_\infty (\|\Phi_{**}^{-1}\|_\infty + \|\Phi_*^{-1}\|_\infty) \|\Sigma_\varepsilon\| \mathbb{Q}(c_0, \Sigma_\varepsilon) \sqrt{dp^2/N} \leq 1/2. \quad (63)$$

Let $N^* = \max\{N_1(\tau), N_2(\tau)\}$. Combining (62) and (63), for $N > N^*$, the following holds,

$$\mathcal{I}_1 + \mathcal{I}_2 + \mathcal{I}_3 \leq -M_\tau + \kappa \|c_0\|^2 + \{2\|\Sigma_\varepsilon\| \mathbb{Q}(c_0, \Sigma_\varepsilon)^2 dp^2/N + 1\}/\lambda_{\min}(X'X/N). \quad (64)$$

Thus,

$$\begin{aligned} & \frac{\mathbb{P}_0(\Phi_{**} \mid y, X)}{\mathbb{P}_0(\Phi_* \mid y, X)} \\ & \leq H(X, \tau) \exp\{-M_\tau + \kappa \|c_0\|^2 + \{2\|\Sigma_\varepsilon\| \mathbb{Q}(c_0, \Sigma_\varepsilon)^2 dp^2/N + 1\}/\lambda_{\min}(X'X/N)\}, \end{aligned} \quad (65)$$

where $H(X, \tau)$ is the bounded function in (42).

For any $\eta > 0$, we have,

$$\begin{aligned} & \mathbb{P}_0\left(\frac{\mathbb{P}_0(\Phi_{**} \mid y, X)}{\mathbb{P}_0(\Phi_* \mid y, X)} > \eta\right) \\ & \leq \mathbb{P}_0(\lambda_{\min}(X'X/N) < \lambda_1) + \mathbb{P}_0\left(\frac{\mathbb{P}_0(\Phi_{**} \mid y, X)}{\mathbb{P}_0(\Phi_* \mid y, X)} > \eta, \lambda_{\min}(X'X/N) > \lambda_1\right) \\ & \stackrel{(a)}{\leq} \mathbb{P}_0(\lambda_{\min}(X'X/N) < \lambda_1) \\ & \quad + \mathbb{P}_0(H(X, \tau) \exp\{-M_\tau + \kappa \|c_0\|^2 + \{2\|\Sigma_\varepsilon\| \mathbb{Q}(c_0, \Sigma_\varepsilon)^2 dp^2/N + 1\}/\lambda_1\} > \eta), \end{aligned} \quad (66)$$

where (a) is due to (42) and the condition $\lambda_{\min}(X'X/N) > \lambda_1$.

By Proposition 1, the first term on the right hand side of (66) is less than $2 \exp\{-\sqrt{Np}\}$. Consider the second term on the right hand side of (66). First note that $\kappa \|c_0\|^2 + \{2\|\Sigma_\varepsilon\| \mathbb{Q}(c_0, \Sigma_\varepsilon)^2 dp^2/N + 1\}/\lambda_1$ and $H(X, \tau)$ are bounded given c_0, Σ_ε and τ . Also, we know $M_\tau \rightarrow \infty$, as $\tau \rightarrow 0$. Therefore for η given above, there exists sufficiently small $\tau = \tau(\eta)$ such that

$$H(X, \tau) \exp\{-M_\tau + \kappa \|c_0\|^2 + \{2\|\Sigma_\varepsilon\| \mathbb{Q}(c_0, \Sigma_\varepsilon)^2 dp^2/N + 1\}/\lambda_1\} \leq \eta. \quad (67)$$

which guarantees $\mathbb{P}_0\left(\frac{\mathbb{P}_0(\Phi \mid y, X)}{\mathbb{P}_0(\Phi_* \mid y, X)} > \eta, \lambda_{\min}(\frac{X'X}{N}) > \lambda_1\right) = 0$.

Hence, for sufficiently small $\tau = \tau(\eta)$ and $N > N^*(\tau, \eta)$,

$$\mathbb{P}_0\left(\frac{\mathbb{P}_0(\Phi \mid y, X)}{\mathbb{P}_0(\Phi_* \mid y, X)} > \eta\right) \leq 2 \exp\{-\sqrt{Np}\}. \quad (68)$$

B Additional Details about Algorithms

B.1 Tuning of Hamiltonian Monte Carlo Algorithm

With θ in the high posterior region, we are ready to tune the Hamiltonian Monte Carlo sampling.

Note that in the leapfrog scheme, M controls the direction of update; therefore, roughly speaking, to make each proposed θ stay inside the high posterior density region, it makes sense to let M scale with the posterior covariance (Gelman et al., 2013). Although the covariance is not available, we can use marginal observed Fisher information at θ^0 , to calculate an approximation. Specifically, we set $M^{-1} = \text{diag}\{\partial^2 U(\theta)/(\partial\theta_i)^2|_{\theta=\theta_0}\}$. For the step size ϵ and the leapfrog steps L , we use the No-U-Turn Sampler (Hoffman and Gelman, 2014)] to automatically adapt these two parameters, so that the algorithm has an acceptance rate around 60%.

B.2 Calculation of the Tree Rank

We have been focusing on *regularizing* the graph estimates using the tree rank. On the other hand, when given an undirected graph \bar{G} , one may be interested in directly *calculating* the tree rank. This is not only useful for properly setting up our simulations later, but also of independent interests. Therefore, we briefly review the relevant results and provide a simplified algorithm.

For a given covering $\bigcup_{l=1}^m T^l \supseteq \bar{G}$, we can remove some edges from each tree, starting from deleting edges not found in \bar{G} , $F^1 = T^1 \cap \bar{G}$, then sequentially for $l = 2, \dots, m$, removing edges previously covered, $F^l = \{T^l \setminus (\bigcup_{h=1}^{l-1} F^h)\} \cap \bar{G}$. Each obtain graph F^l is known as a “forest”, an acyclic graph with possible disconnectivity. It is not hard to see that $\bar{G} = \bigcup_{l=1}^m F^l$, $F^l \cap F^h = \emptyset$ for any $l \neq h$; further, the tree rank is exactly equal to the minimum covering number using forests. Using

$$\text{Tree-Rank}(\bar{G}) = \max_{H \subseteq \bar{G}} \left\lceil \frac{|E_H|}{|V_H| - 1} \right\rceil,$$

we can maximize over all subgraphs of \bar{G} which has cardinality of $O(2^p)$, efficient search algorithm such as Gabow and Westermann (1992) has been developed. Briefly speaking, their algorithm is a combination of solving k -forest problems (covering as many edges in \bar{G} as possible using k forests) and a binary search for the minimum k that covers all the edges in \bar{G} . Due to the high complexity, we refer the readers to that article for the details. In the meantime, we present an approximate algorithm that is much easier to implement.

Let W^1 be a $p \times p$ weight matrix with $W_{i,j}^1 = 1$ if $(i, j) \in \bar{G}$, and $W_{i,j}^1 = 0$ otherwise.

Let W^1 be a $p \times p$ weight matrix with $W_{i,j}^1 = 1$ if $(i, j) \in \bar{G}$, and $W_{i,j}^1 = 0$ otherwise.

Algorithm 1. Find an upper bound estimate $m \geq \text{Tree-Rank}(\bar{G})$.

while $W^l \neq O$ **do**

 Find the maximum spanning tree of a complete graph with weight matrix W^l , denote

 the produced tree by T^l and its adjacency matrix by A_{T^l} ;

 Set $W^{l+1} = W^l \circ (J - A_{T^l})$;

 Set $l \leftarrow l + 1$;

Set $m = l - 1$.

In the above, O denotes the $p \times p$ matrix filled by zeros, and J the matrix by ones; and one can use Prim's algorithm to easily find the maximum spanning tree (Prim, 1957).